TECHNICAL MEMORANDUM

X-87

EXPERIMENTAL PERFORMANCE OF LIQUID HYDROGEN AND LIQUID

FLUORINE IN REGENERATIVELY COOLED ROCKET ENGINES

By H. W. Douglass, G. Hennings, and H. G. Price, Jr.

Lewis Research Center
Cleveland, Ohio
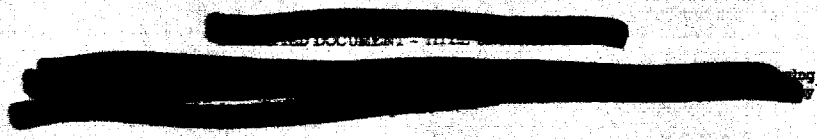
NATIONAL AERONAUTICS AND SPACE ADMINISTRATION

WASHINGTON   November 1959

NATIONAL AERONAUTICS AND SPACE ADMINISTRATION

TECHNICAL MEMORANDUM X-87

EXPERIMENTAL PERFORMANCE OF LIQUID HYDROGEN AND LIQUID FLUORINE

IN REGENERATIVELY COOLED ROCKET ENGINES*

By H. W. Douglass, G. Hennings, and H. G. Price, Jr.

33342

SUMMARY

The rocket propellant combination hydrogen-fluorine gave very high performance efficiency (98%) when burned in a 5000-pound-thrust rocket engine at a combustion pressure of 300 pounds per square inch absolute. A maximum specific impulse of 352 pound-seconds per pound was obtained for a combination with 13.8 percent hydrogen. This value is 98 percent of the maximum theoretically possible in the particular thrust chamber used, considering equilibrium expansion to sea-level pressure. With 6.1 percent fuel, where propellant bulk density is greater, a specific impulse of 314 pound-seconds per pound was measured. Two different injectors gave similar results.

Complete regenerative cooling with hydrogen was successful, even though average over-all heat-transfer rates (4.5 to 8.5 Btu/(sec)(sq in.)) greatly exceeded those encountered with conventional propellants. Because pronounced changes in hydrogen density occur in the coolant passages, automatic control of propellant flow rates was employed to ensure proper mixture ratios.

No problems were apparent relative to engine operation, starting, or combustion stability.

INTRODUCTION

Theoretical studies show that the rocket propellant combination hydrogen-fluorine has the highest performance potential of all stable chemical sources of energy (ref. 1). Furthermore, heat-transfer analyses indicate that hydrogen can exceed all other rocket propellants as a regenerative coolant (ref. 2). In addition to having high heat capacity, hydrogen is free of the physical limitations of certain other fuels when they are used as coolants (e.g., coking and decomposition). Even boiling can be readily avoided by using the hydrogen above its critical pressure, which is only 188 pounds per square inch absolute.

---

*Title, Unclassified.

Because of the absence of experimental data, the objectives of the present work were (1) to measure the performance of hydrogen-fluorine in an experimental rocket engine, (2) to determine whether such an engine could be regeneratively cooled by the hydrogen, and (3) to explore for problem areas associated with the use of hydrogen-fluorine in rocket engines.

The experimental 5000-pound-thrust rocket engines used for the investigation were operated at a nominal combustion pressure of 300 pounds per square inch absolute. The data cover propellant mixtures ranging from 6 to 20 percent fuel. Specific impulse, characteristic velocity, nozzle thrust coefficient, and heat rejection were determined as functions of oxidant-fuel ratio. This work was done at the NASA Lewis Research Center.

A construction method for lightweight rocket thrust chambers is described in appendix A, by Edward F. Baehr.

COMBUSTION-CHAMBER DESIGN

Injectors

Both a showerhead-type and a triplet-type injector were used in this initial study. Showerhead injectors generally give stable combustion with relatively low heat rejection to the engine walls and minimum chance of injector burnout. Since neither atomization nor mixing of the propellants is provided by these injectors, showerhead injectors have resulted in lower performance than other types when used with conventional rocket propellants. When used with hydrogen-oxygen, however, showerhead injectors have been found to give high performance (ref. 3).

The triplet injector was tested to ascertain the influence of propellant preparation on combustion efficiency for the highly reactive hydrogen-fluorine propellant combination. The triplet arrangement of two fuel jets impinging on one oxidant jet serves to enforce mixing and rapid dispersion of propellants in the combustion chamber. With other propellants, the use of triplet-type injectors has resulted in significant improvement in performance and has given good results in small-scale studies with gaseous hydrogen and liquid oxygen (refs. 4 and 5).

The two injectors used for this hydrogen-fluorine work are illustrated in figure 1. Both have the same arrangement of propellant holes on the injector face; they differ only in the characteristics of the basic injection elements. For both injectors, the fuel holes are 0.067 inch in diameter and the oxidant holes are 0.043 inch. The injectors are designed for use at the oxidant-fuel proportions of maximum theoretical performance; this specifies that 15 percent of the propellant combination
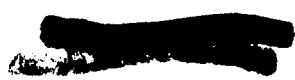
is fuel. At these conditions, oxidant is injected at a velocity near 100 feet per second, and the fuel injection velocity is about 1700 feet per second. The half-angle of impingement between fuel holes in the triplet arrangement is 15°, and the point of impingement is 0.575 inch from the injector face. Impinging triplet-jet elements are arranged so that the resulting spray fans form a noninterference grid across the face, as indicated in figure 1. If two fuel holes and one oxidant hole are considered to compose the elemental unit of these injectors, then engine thrust per injection element is 39 pounds.

In addition to atomization and mixing, propellant distribution by the injector is an important design consideration. Here, propellant distribution is arranged to be uniform across the injector face, and in fine detail. That is, there are many propellant orifices; each of the oxidant holes is surrounded by fuel holes.

Fineness of distribution makes for better performance. It also provides more uniform cooling of the injector face. Figure 2 illustrates the technique of using the fuel to cool these injectors. Hydrogen enters the injector from the coolant jacket of the engine. It then flows through holes in the coolant distribution plate. These holes are so spaced that the hydrogen sweeps the back side of the injector face before arriving at the holes, which deliver it to the combustion chamber.

Fluorine enters a manifold formed by a dome attached to the injector (located left of the manifold plate in fig. 2) and then flows through delivery tubes and orifices into the combustion chamber. The delivery tubes, the coolant distribution plate, and the injector face plate are made of copper; the fluorine manifold plate is made of stainless steel. The entire structure is put together by furnace-brazing.

The assembly of an injector with a thrust chamber is illustrated in figure 3. The centerbody of the injector and the fluorine manifold dome are clamped to the thrust chamber by flange pieces. Outside sealing is accomplished with Teflon-coated self-pressurizing metal O-rings; a double O-ring seal is used at the fluorine manifold, with helium pressurization between rings. The internal seal between hydrogen passages and the combustion zone consists of a tapered metal-to-metal joint mated under compression.

Thrust Chambers

The thrust chambers used were designed to develop 5000 pounds of thrust at sea level when operated at a combustion pressure of 300 pounds per square inch absolute. The nozzle expansion area ratio is 3.68; chamber contraction area ratio is 1.89; throat diameter is 3.91 inches. The length from injector to throat is 12 inches, and the chamber characteristic length is 20 inches. The divergent portion of the nozzle is conical, with a 15° half-angle.
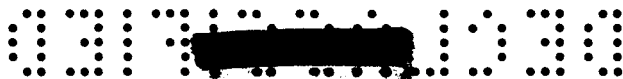
The thrust chambers were made from 72 longitudinal channels that were bundled together, wire-wrapped, and brazed (fig. 4). The 72 longitudinal channels are U-shaped in cross section and are made of nickel 0.020 inch thick. Such thin walls are necessary for adequate cooling. Since these channels provide passageways for the coolant, the height of the channels is an important design consideration. The fabrication details are given in appendix A.

For cooling, the hydrogen enters the coolant passageway at the exit end of the nozzle and flows toward the injector. At this time, changes in hydrogen temperature and pressure are expected to cause the density to change by a factor of about 50. The coolant channel height had to be tailored to match this changing hydrogen density from one end of the combustion chamber to the other. The design of this tapering channel height was arrived at by calculating local heat-transfer rates with the aid of electronic computing equipment (ref. 2). The design was to provide a maximum gas-side wall temperature of 1000° F when the engine is operated with 15 percent hydrogen in the propellant combination. A complete listing of combustion-chamber and coolant-passage dimensions is given in table I.

EXPERIMENTAL FACILITIES

The propellant systems, thrust stand, instrumentation, controls, and related apparatus are shown in figures 5 to 9. These facilities and the experimental procedure are described in appendix B.

RESULTS AND DISCUSSION

Performance

All experimental performance data are listed in table II. Pertinent theoretical performance values corresponding to the experimental conditions are included in the table. Symbols are defined in appendix C.

Experimental performance values were so high compared with the ideal theoretical values reported in reference 1 that it was desirable to compare actual performance with the maximum theoretically possible for the real engine configuration and operating conditions used. Consequently, the ideal theoretical calculations were modified to include divergence losses in the nozzle and momentum pressure drop in the combustion chamber and to account for the specific combustion and exit pressure conditions for each run (see appendix C). Actual specific-impulse values plotted in figure 10(a) reach as high as 98 percent of the highest theoretically possible with the particular thrust chamber used.
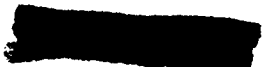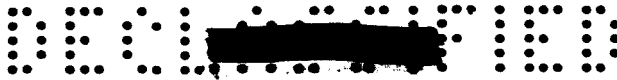
The eleven operating conditions ranged from nearly 20 to about 6 percent fuel in the propellant combination. The maximum specific impulse, from measurements near 14 percent fuel, was 352 pound-seconds per pound; the experimental specific impulse dropped to 314 at 6.1 percent fuel. These values correspond to vacuum specific-impulse values of 397 and 354, respectively, for the present engines, which had a 3.68 expansion area ratio.

Performance at fuel-oxidant proportions near stoichiometric, 5 percent fuel, is of considerable interest if the use of hydrogen is to be minimized. The extremely low density of hydrogen requires that its tanks, pumps, valves, and pipes be relatively large. Operation at less than 14 percent fuel, although resulting in lower specific impulse, may represent a reasonable compromise in performance to reduce fuel requirements.

Fortunately, the theoretical peak specific impulse, assuming shifting equilibrium expansion, occurs at lower proportions of fuel as the nozzle expansion ratio increases. This would pertain, for example, to engines designed to exhaust into a high-altitude environment (near-vacuum) and, to a more limited extent, to pump-fed engines intended for operation at high chamber pressures in low-altitude environments. The deciding factor depends upon whether expansion of the combustion products through the nozzle is more closely related to frozen or to shifting equilibrium conditions. This can be more clearly expressed by reference to figure 11, where theoretical curves of specific impulse are presented for frozen and equilibrium expansion across high pressure ratios.

If equilibrium expansion prevails, 6 percent fuel in the propellant combination may be appropriate for application to space flight; then the bulk density of the combination will be 43.55 pounds per cubic foot, or nearly double that at 14 percent fuel. Actually, the experimental performance of hydrogen-fluorine apparently did exceed the frozen values under most conditions, and the curve has the same shape as the curve for shifting equilibrium.

Performance efficiencies, in terms of percentage of the values theoretically possible with the particular engine used, are presented in figure 10(a). As indicated by these plots, the experimental specific-impulse values surpassed the calculated ones for frozen expansion throughout most of the range studied, in some cases by as much as 3 percent. Experimental specific-impulse data held at 98 percent of corresponding theoretical data for shifting equilibrium expansion except at fuel-oxidant proportions having less than 11 percent fuel, where efficiency dropped.

Experimental characteristic velocity and nozzle thrust coefficient are referenced against theoretical data in figures 10(b) and (c). Experimental thrust-coefficient efficiency remained high, while characteristic-velocity efficiency dropped at propellant proportions

having less than 11 percent fuel. Therefore, a decrease in characteristic velocity was apparently responsible for the corresponding drop in specific impulse.

Since characteristic velocity remains unchanged when engine pressure ratio varies, the drop in this efficiency at the lower fuel percentages (which are of the greatest interest for high-pressure-ratio engines) is significant. Possibly this efficiency can be improved by variation of the propellant injection technique. It may be noted, however, that in the present work no distinction can be made between results from the showerhead injector and those from the triplet.

Regenerative Cooling

The capability of hydrogen to completely cool the engines regeneratively was successfully demonstrated. In figure 12, values of average over-all heat flux per unit area are plotted as a function of the percentage fuel used in the propellant combination. The top curve represents the heat transfer anticipated by design computations, assuming 100-percent combustion efficiency. The lower curve resulted from calculations based on the actual equilibrium performance efficiencies experienced, as indicated for characteristic velocity in figure 10(b). The data points in figure 12 represent the average heat transfer through the engine walls as measured experimentally. These calculated and measured values are in reasonable agreement, considering the assumptions necessary in the design analysis.

The first run was made near 20 percent fuel; successive runs were made using less fuel, until proportions near stoichiometric were reached. Cooling becomes more difficult, of course, as stoichiometric proportions are approached, assuming combustion efficiency remains constant.

After runs near 6 and 7 percent fuel, there were indications that the engine inner walls had begun to melt or burn slightly at the centers of the channels in four rather well-defined areas (fig. 13). These areas were related in position to four portions near the edge of the injector that could provide propellant mixtures leaner in fuel than other locations. It is supposed, then, that the engine walls were damaged by localized oxidant-rich combustion. Such localized conditions could undoubtedly be alleviated by injector modification during engine development. Even with the channel walls slightly damaged, the engine continued to perform satisfactorily for the test period.

The engine coolant passages were designed for use at propellant proportions of about 15 percent fuel. Even when less fuel was employed with this design, calculations indicated wall temperatures (assumed uniform circumferentially) that were well below the melting point of

nickel, of which the walls were made. Modification of the coolant-passage design would permit some control of wall temperatures as compromised by coolant pressure drop, but would not significantly affect the total heat-transfer rate, since this rate is determined primarily by combustion-gas conditions.

The results of cooling design analysis and measurements made during the experimental runs are listed in detail in table III. It is apparent from these data that a very broad range in hydrogen density must be taken into account. Thus, careful cooling design is required to afford an acceptable balance between wall temperature and coolant pressure drop.

Operations

The extreme sensitivity of the density of hydrogen to environmental conditions can cause cooling troubles. For example, the flow rate of hydrogen through the longitudinal coolant passages depends upon the cross-sectional area of the passages, the differential pressure available from one end to the other, and the fluid density. As indicated previously, values were assigned to these parameters by design calculations. However, in those calculations, certain assumptions were necessary with respect to combustion efficiency, local heat-transfer coefficients, coolant-flow velocities, friction factors, and so forth, that could lead to design errors. If a design error caused a fuel-flow rate to be too low relative to the oxidant-flow rate in the engine, the combustion temperature would be higher than had been anticipated, and heat-transfer rates would be higher. The coolant temperature would exceed that expected. Hence, the density of the hydrogen (coolant) would be decreased appreciably, and its mass-flow rate would drop accordingly. This decrease in flow rate would further alter the oxidant-fuel ratio in the combustion chamber, creating even higher temperatures and thus propagating the cycle.

It was for this reason that automatic flow-control valves were considered essential. These controls very successfully held oxidant-fuel ratio at the desired point by adjusting to the demands of the run.

Throughout the experimental program no combustion instabilities were encountered, nor was any difficulty experienced with engine starting or shutdown.

SUMMARY OF RESULTS AND CONCLUSIONS

The following results were obtained from an experimental investigation of a regeneratively cooled hydrogen-fluorine rocket engine:

1. Hydrogen and fluorine were successfully burned at high efficiency over a range of 6 to 20 percent fuel in 5000-pound-thrust rocket engines operating at a combustion pressure of 300 pounds per square inch absolute and exhausting to atmospheric pressure.

2. Maximum specific impulse was 352 pound-seconds per pound at 13.8 percent fuel. This value is 96.5 percent of the maximum ideal theoretical shifting equilibrium value and 98 percent of the maximum theoretically possible with the chamber geometry actually used.

3. The specific impulse at 6 percent fuel was 314 pound-seconds per pound, or 91 percent of that theoretically possible with the real engine.

4. The corresponding vacuum specific-impulse values would be 397 and 354, respectively, for the 3.68-area-ratio engine used.

5. Two different injector types, a showerhead and a triplet, gave similar results.

6. Regenerative cooling with hydrogen was successful. Experimental cooling loads agreed reasonably well with design expectations.

7. Average over-all heat-flux values ranged from 4.5 to 8.5 $Btu/(sec)(sq in.)$.

8. Automatic control of oxidant-fuel ratio was found highly desirable, and probably essential, for regeneratively hydrogen-cooled thrust chambers.

9. No starting, operational, or combustion stability problems were uncovered.

The high performance and successful cooling in small rocket engines indicate that large engines can be developed that can burn hydrogen-fluorine at equally high performance levels and that can be adequately cooled by the hydrogen even with large nozzle expansion ratios.

Lewis Research Center
    National Aeronautics and Space Administration
        Cleveland, Ohio, June 10, 1959
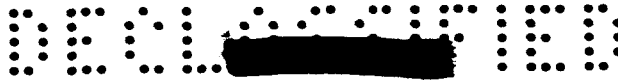
APPENDIX A

CONSTRUCTION METHOD FOR LIGHTWEIGHT ROCKET THRUST CHAMBERS[1]

By Edward F. Baehr

Research on the use of high-energy liquid propellants requires rocket thrust chambers capable of withstanding very high heat-flux rates. In order to meet this need, thin-gage, high-conductivity metal must be used for the inner surface of the chamber. To carry the heat away rapidly from the thin metal, the velocity of the coolant must preferably be tailored to the local conditions.

The NASA Lewis Research Center has developed a wire-wrapped channel construction technique that gives complete freedom in the coolant-passage area distribution and is suited for use with extremely light-gage metals. Since this method of fabrication may be useful for flight-type thrust chambers, gas generators, or any other device requiring these features, as well as for experimental rocket thrust chambers, a brief description of the fabrication technique is presented.

Fabrication Procedure

The technique described herein consists of the following steps:

(1) Making the channels

(2) Assembling the channels

(3) Brazing the channels

(4) Sizing the channel heights

(5) Wire- or ribbon-wrapping

(6) Brazing the wrapping

(7) Installing manifolds and flanges

(8) Heat-treating

Making the channels. - The operation of cutting the light-gage sheet-metal strips for the channels of the engine is shown in figure 14. The blanking dies used to cut the material were simple steel-rule type mounted in heavy steel frames and cast in place with Cerromatrix metal.

_____
[1]Patent applied for.
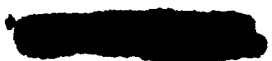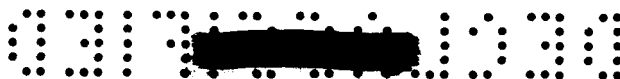
These dies were set for zero clearance to produce burr-free edges on the light-gage metal.

The flat blank strips were then hand-curved to the approximate shape of the engine contour and placed in a simple die mounted in a press brake, where they were formed to the channel cross section (fig. 15). Figure 16 shows the dies used to form the channels. The female die was made of three-piece construction so that slight tailoring could be very easily accomplished by removing the center portion for rework. The center portion of the female die was made up of a part whose narrow side had the contour of the inside of the engine and whose sides represented radial planes through the engine centerline. The two side portions of this female die merely enclosed this shape and had a convenient projection in height beyond the inner contour to form channels of the appropriate height.

The male portion of the die was of one-piece construction representing the angular segment of the engine with thickness allowance on the sides and bottom relative to the female die. This means that the sides of all dies represented radial plane surfaces. The only contours were those required to form the various diameters of the engine. No attempt was made to form a curved circumferential surface, but rather a flat chord was used for simplicity.

To facilitate removal of the rather delicate channel section from the die, a hydraulic pressure cell was introduced into the die holder, along with the three-piece channel die, so that the female die could be opened to remove the channel section. Experience indicated that tooling designed to produce channels approximately 0.002 inch undersize was desirable to ensure proper fit of the completed chamber around a brazing mandrel. It has also been noted that this type of die has a tendency to coin the channel slightly as the die is bottomed, resulting in less than the designed angular flare to the channel sides. This, however, has been an advantage, in that it facilitates close fitting during the subsequent spot-welding procedure.

Assembling the channels. - After the proper number of channels were formed, they were assembled around the brazing mandrel. Small wood blocks were placed in the channels to permit clamping the inner surfaces in contact with the mandrel. A channel assembly clamped to the brazing mandrel is shown in figure 17. The number of clamps used depended on the size of the engine and the fit of the channels on the mandrel.

The channels were next spotwelded together (fig. 18) for the brazing operation that followed. The spotwelds ensured that there would be no slipping as the assembly was heated for the brazing operation.
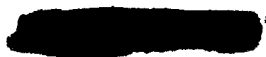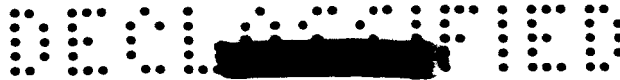
Brazing the channels. - A number of different techniques have been successfully used for brazing the channels together. One chamber was brazed using copper wire placed in the grooves between channels on the combustion-chamber inner surface. Subsequent assemblies have been made using commercial brazing powders applied to the outside edge of the ribs. Figure 19 shows the application of a powdered braze alloy slurry to the ribs of the channels. Care must be exercised in the application of this braze alloy to prevent excess braze from flowing onto cooling surfaces. For the most uniform results, vacuum-brazing has been used, but hydrogen-brazing has also been successful. It has been the practice to be very conservative in the application of braze alloys. This has resulted in an occasional rerun being required to complete the brazing of all channels.

Sizing the channel heights. - The actual cooling-passage geometry required for the engine was provided by grinding the channel ribs to the appropriate heights along the length of the combustion chamber. Although the original blank included approximately the right metal allowances for rib height, a nominal 0.030 inch was included for final sizing operations. In order to size these passage heights accurately, the brazed channel assembly was removed from the brazing mandrel and transferred to an accurately machined aluminum mandrel for the grinding operation, as shown in figure 20. On the early chambers, dry-grinding was used to size the ribs while rotating the channel assembly in a contour lathe. However, some difficulty was experienced in getting accurate contours for the individual channels by this technique. To improve accuracy and to speed the metal removal rate, electrolytic grinding has since been used very successfully. In this latter technique a simple mechanical means has been employed to control channel height relative to the engine wall automatically.

Wire- or ribbon-wrapping. - After the channel heights were ground to size and inspected, the engine was removed from the machining mandrel and transferred once again to the brazing mandrel for the wire-wrapping process. The first chambers were built with round wire wrapped in spiral grooves ground across the ribs of the engine. Later engines have been built using square wire or formed ribbon wrapped on smooth engine ribs. This wrapping was accomplished in a lathe using a friction device to provide the wrapping tension (see fig. 21).

When round wire was used, the lead of the spiral groove was greater than the cross-sectional diameter of the wire, to provide a braze allowance between wires. This allowed proper flow of the braze to the joint between wire and rib. When square wire was used, the wire was fed through a set of rollers, as part of the wrapping operation, to provide small projections on one side of the wire for proper spacing. For the braze alloys used, 0.004- to 0.005-inch spacing was suitable.

When wrapping the grooved channels with round wire, it was possible to start at either end of the chamber and wrap directly to the other
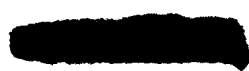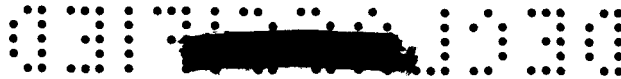
end, since the groove prevented the wire from slipping along the contour. However, when square wire was used on smooth ribs, the wrapping was started at the throat of the engine and could proceed in either direction from that station. To complete the second half, the wire was then welded on at the throat and wrapped in the opposite direction. The wires were secured at both ends by tack-welding to the ribs.

Brazing the wrapping. - The wrapped chamber on the brazing mandrel was prepared for furnace-brazing by painting the powdered braze alloy slurry on the outside surface of the wires as shown in figure 22. Here again care was taken that excess braze alloy would not be permitted to flow to undesired regions of the engine. This occasionally necessitated a second brazing cycle to completely seal the wire wrap. These brazing operations were usually accomplished in a high-vacuum brazing furnace. A thrust chamber is shown being placed in the brazing furnace in figure 23.

Installing manifolds and flanges. - The brazed assembly was next reinstalled on the machining mandrel and put into the contour lathe for trimming and grinding operations at both ends of the chamber. The exit end of the chamber was made ready for the installation of the fuel inlet manifold, and the injector end was ground for the mounting flange. This flange and the fuel inlet manifold were then fitted and brazed in place with the inner portion of the ribs open for visual inspection. A ring was next fitted to the ribs and manifold as a closure. These miscellaneous parts are shown in figure 24.

The remaining step was to install the injector seal ring at the end of the ribs. To do this the engine was mounted in the lathe without a mandrel so that an internal grinding operation could remove a portion of the ribs at the injector end. A small slotted seal ring was fitted to the ends of the ribs. After being brazed in place, the seal surface of this ring and surfaces of the injector flange were machined at one setup. The injector flange was gaged so that various thrust chambers and injectors were interchangeable. Figure 25 shows the seal ring and cooling-jacket discharge passages.

Heat-treating. - The completed engine was then heat-treated to increase the yield strength of the wire-wrapped material. The thrust chambers built to date by this laboratory have used Allegheny Ludlum AM 350 stainless-steel wire wrapping that is heat-treated by a cold treatment at -100° F for 3 hours followed by 3 hours at 850° F. This operation triples the yield strength of the wire wrap without affecting the properties of the ribs or the flanges. Figure 26 shows a completed chamber.

Pressure-checking. - The completed chamber was hydrostatically tested to 2 times operating pressure to ensure adequate strength of all brazed
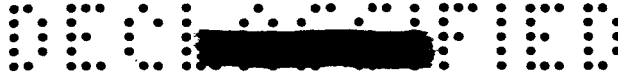
joints. This also served as a leak check on the entire structure. Tests were made with a sample cylinder, $7\frac{1}{2}$ inches in diameter, constructed of 76 channels of 0.020-inch annealed nickel. The channels were wire-wrapped with soft steel wire and copper-brazed. Theoretically, these channels would have yielded as edge-supported flat plates at about 300 pounds per square inch and would have failed as stretched membranes at about 1060 pounds per square inch. The tests resulted in first permanent deformation at over 1000 pounds per square inch and no failure of channels or brazed joints up to 6000 pounds per square inch.

Discussion

The preceding description tells of the steps used in the manufacture of a research-type thrust chamber. This chamber used single-pass counter-flow cooling. However, a flight-type chamber would include a different type of inlet manifold and injector flange. Perhaps an integral injector would be used. The inlet fuel manifolds for flight-type engines probably would be of formed sheet-metal construction. For minimum engine weight, the fuel inlet manifold should be located near the throat of the engine rather than at the large exit diameter. The fluid might be conducted to the exit end of the engine in "piggyback" channel passages or in a two-pass configuration from the manifold to the exit end and then returned the length of the engine to the injector. For a truly flight-type article, a future refinement that could easily be applied is a grading of the wire wrap along the length of the chamber to match the strength requirements consistent with the internal pressure profile.
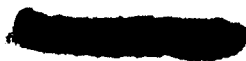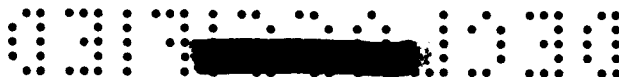
APPENDIX B

APPARATUS AND PROCEDURE

Propellant Flow Systems

Oxidant. - The fluorine flow system is illustrated schematically in figure 5. In this system the fluorine tank and the entire flow line, to within about 2 feet of the thrust chamber, were surrounded by liquid nitrogen during operation. Since the boiling point of nitrogen is lower than that of fluorine, the use of liquid nitrogen affords the safest and most convenient way to handle fluorine; further, a bath of liquid nitrogen improves the ease and reliability of fluorine flow-rate measurement by ensuring constant temperature and hence constant density.

Located in the fluorine main flow line were two remotely operated valves. One, near the tank, was simply an emergency shutoff valve, pneumatically controlled. The main fire valve was located near the thrust chamber. This hydraulically operated valve served to control oxidant-flow rate precisely during experimental firings. The fluorine valves were of a packless, bellows-seal type with metal seats and plugs.

All valve connections were made with serrated flanges and aluminum gaskets. Threaded connections and sleeve joints were avoided because crevices inherent in them could contain contaminants capable of reacting with the fluorine and causing destruction of the system. Whenever possible, pipe connections in the fluorine system were welded. A special welding technique was worked out that consisted of V-joint welding by a heliarc technique with inert gas inside the pipe being welded. This procedure was followed to eliminate slag inclusion in the welds. After welding was completed, each joint was X-ray photographed as a check on weld penetration. Except for some stainless-steel valve bodies and a nickel flowmeter, the entire fluorine system was fabricated of monel.

Fuel. - The hydrogen flow system is illustrated in figure 6. The main hydrogen flow line was insulated with foam glass. The liquid-hydrogen tank was inside an evacuated jacket, which in turn was surrounded by a liquid-nitrogen radiation shield; a final vacuum jacket surrounded the whole assembly. The hydrogen vent line for this tank was run a considerable distance away from the test cell to prevent fire and flashback.

The hydrogen flow line also had two main valves, an emergency shutoff and the automatic flow control valve; but in addition, there was a bypass valve to permit flow of liquid hydrogen to cool the main flow line before the engine was operated. Hydrogen valves were Teflon packed and had Teflon seats with metal plugs.
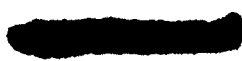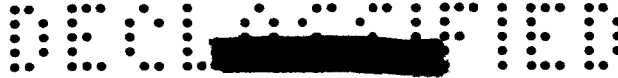
Valve connections consisted of serrated flanges for convenience. Pipe connections were made by conventional techniques for flow systems. Except for the brass flowmeter, all metal components were of stainless steel.

Exhaust-Gas Scrubber

The operation of hydrogen-fluorine engines generates toxic combustion products, principally hydrogen fluoride. A rocket exhaust-gas scrubber (fig. 7) was used to remove these toxic products.

Flame from the rocket engine passed through the spokes of a wheel-like manifold in the scrubber. These spokes introduced water directly into the core of the flame and greatly reduced the exhaust-gas temperatures and velocities. The gases were then fed along the horizontal duct into the vertical section. Upon entering the vertical section, the gases were exposed to water sprays from hundreds of nozzles arranged in seven tiers. The gases were scrubbed by this water, which flowed at about 8400 gallons per minute. The resulting hydrofluoric acid solution was collected in a sump pit at the bottom of the vertical section.

The use of the scrubber presented a problem in using hydrogen. Since the operations of the engine were conducted by using a hydrogen lead and override and by running fuel-rich, excess hydrogen could easily collect and mix with air in the scrubber ducts. If this should occur, an explosion would be inevitable when the engine fired. Therefore, the entire scrubber had to be inerted by replacing all the air with carbon dioxide. This led to the further requirement of monitoring the oxygen content at various stations in the scrubber. No rocket runs were made unless sampling showed less than 3 percent oxygen concentration at each monitoring station.

Thrust Stand

The experimental thrust chamber was mounted horizontally on a floating bed, suspended by four flexure plates from the main structural frame of the thrust stand (fig. 8). Thrust was measured by a single transducer located on the centerline of the combustion chamber behind the floating bed. Calibration was accomplished by means of a standard transducer mounted temporarily between the thrust stand and an independently supported rigid post.

E-183
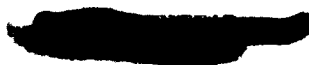
Instrumentation

In addition to thrust, the parameters measured included combustion pressure, oxidant- and fuel-flow rates, hydrogen temperatures and pressures, and the temperature and pressure differentials across the coolant passage. All measurements, except those of temperatures, were made with strain-gage-type primary transducers. Signals from these transducers were fed to voltage amplifiers, which were adjusted to cover each full measured input range with an output span of 0 to 1 volt. Generally, the output signal from each amplifier was split to drive both a direct-inking strip-chart recorder and one galvanometer element of a multichannel photographic oscillograph. Additional splitting of flow-rate and combustion-pressure signals supplied information to the automatic flow-control valves.

Fluorine-flow rate was measured by recording the differential pressure across a Venturi in the main flow line. This measurement is dependent on fluid density. By immersion of the entire fluorine system in liquid nitrogen, the fluorine temperature was kept constant and thus density was constant.

The Venturi for measuring hydrogen-flow rate was located at the bottom of the dip tube in the hydrogen tank. During run conditions, this was the only location at which the hydrogen temperature, pressure, and consequently density, were constant and reproducible. Coolant temperature rise was measured by differential copper-constantan thermocouple pairs across the coolant passage and by single thermocouples referenced against the temperature of boiling liquid nitrogen. In addition, absolute temperatures of liquid hydrogen were measured at the engine coolant inlet manifold and in the hydrogen tank by use of calibrated carbon resistors. The resistance of these elements changes markedly with temperature in the region of the hydrogen boiling point. Several such elements, located at 1-foot intervals along the hydrogen tank dip tube, indicated the liquid level at any time.

All primary transducers were calibrated against standard instruments before installation. Further checks were made following installation by applying known loads to be read through each complete measuring and recording channel. As a result, the instrumentation used for this program provided measurements having probable errors of less than 1 percent.

Controls

Automatic servo-operated flow control valves were installed in both the fuel and oxidant flow lines. These valves functioned so that the
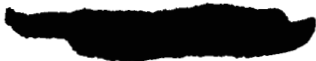
fuel-flow rate was controlled to hold the proper combustion pressure, and the oxidant flow was proportioned to the actual fuel flow. By using suitable timing devices, several different oxidant-fuel ratios could be obtained in a stepwise fashion during a single firing. Control signals came from the primary measuring instrumentation.

These valves consisted of commercially available bodies and trims, but were modified by the addition of hydraulic actuators designed at the NASA Lewis Research Center (fig. 9). Electronic control circuitry was also of NASA design (ref. 6). Full stroke travel time of the valves was on the order of 5 to 10 milliseconds. Accuracy of control to a stable specified flow rate was better than 5 percent.

Since the valves operated with closed-loop control, no calibrations were necessary to establish flow-rate relations. Trial runs were made with liquid-nitrogen flow, however, to permit adjustment of the sensitivity and stability of control response.

Working Fluids

Both propellants were obtained, handled, and used in the liquid state. Each propellant was of at least 98 percent purity. The liquid hydrogen was 95 percent in the para form. Helium gas was used for pressurization of the fluorine tank; the liquid-hydrogen tank was pressurized with gaseous hydrogen.

Procedures

Proper cleaning of fluorine systems is essential. The present system was cleaned and passivated by the following procedure. The entire tank and flow line assembly was washed thoroughly with carbon tetrachloride. This was followed by washing with acetone. Then the system was blown dry with nitrogen gas. The next step involved a rinse with 20 percent nitric acid, followed by a water rinse. Then an acetone wash removed the water, and finally Freon 12 was flowed through the complete system to remove the acetone. The system was next purged with dry helium gas. Following this, the entire assembly was evacuated for an extended period of time to remove all traces of condensibles. For complete passivation, fluorine gas was introduced directly into the vacuum and left in the system for 12 hours at a pressure of 50 pounds per square inch. The fluorine system was then ready for use. After each test run, all residual fluorine was removed and the tank was warmed as rapidly as possible with electric heaters. This was done to reduce the possibility of condensing moisture and other contaminants into the tank. During standby between runs, the entire fluorine system, including all flow and

transfer lines, was kept closed and under slight positive helium pressure to exclude entrance of contaminants.

Cleaning requirements for hydrogen systems are not rigorous, but all oxygen must be removed before hydrogen is admitted. This was accomplished by repeatedly evacuating the system and then breaking this vacuum with helium.

Both the hydrogen and the fluorine were transferred to the test-cell tanks as liquids from mobile supply trailers by slightly pressurizing the supply trailers. The transfer systems were prepared and treated in the same manner as the main flow systems. After the experimental runs were completed, any appreciable quantities of fluorine remaining in the tank were returned to the supply trailer. Small quantities of residual fluorine were disposed of by reaction in charcoal burners (ref. 7).

All experimental runs were made with a fuel lead and override to ensure that the engine coolant passages were filled with hydrogen and that the hot metal combustion-chamber wall was not exposed to elemental fluorine. The runs were started with full-rated propellant flows. No external ignition system was required; combustion with fluorine is initiated spontaneously. The duration of each firing was about 14 seconds; generally, this was broken into three sequential run segments, each having a different oxidant-fuel ratio. The run segments, then, were of about 4-second duration each. From observations of the instrument records, conditions within the engines, including heat-transfer rates, were well established within that period.

APPENDIX C

ANALYTICAL PERFORMANCE CALCULATIONS

Experimentally obtained values of specific impulse, characteristic velocity, and nozzle thrust coefficient are often compared with theoretical values. These theoretical values are generally calculated with no momentum pressure loss, no nozzle divergence angle losses, and at an ideal expansion ratio so that exit pressure always equals ambient pressure. Actual engines will have these losses and others of lesser significance. Therefore, unless the theoretical data are adjusted, a misleading evaluation of the experimental data is likely. The method presently described is applicable for adjusting both equilibrium- and frozen-composition theoretical data to a specific experimental run condition by accounting for the primary loss sources mentioned.

Symbols

A   area

C_F thrust coefficient

c^* characteristic velocity

F   thrust

g_c gravitational conversion factor, $32.2 \dfrac{\text{ft-lb mass}}{(\text{sec}^2)(\text{lb force})}$

I   specific impulse

$\dot{m}$ mass flow

P   absolute pressure, total unless indicated otherwise

V   calculated average velocity of unburned propellants

v   velocity of combustion gases

$\dot{w}$ propellant weight flow

α half-angle of nozzle divergence

λ $(1 + \cos \alpha)/2$

Subscripts:

a   ambient

c   combustion chamber

d   corrected for nozzle divergence

e   at nozzle exit

eq   equilibrium

f   frozen

i   at injector

id   ideal

n   at nozzle entrance

R   real engine

s   static

t   at nozzle throat

vac   vacuum

x   experimental

Computational Procedure

Characteristic velocity. - Of the three corrections considered, only the momentum pressure-loss term is applicable to characteristic velocity. Theoretical calculations of characteristic velocity are based on the total pressure $P_{c,n}$ of the combustion gases at the entrance to the nozzle; but, in experimental work, it is generally more convenient to measure the pressure $P_{c,i}$ at the injector, where combustion-gas velocity may be considered negligible. The pressures $P_{c,n}$ and $P_{c,i}$ can be reconciled analytically for momentum loss by the equation (ref. 8, p. 17)

$$P_{c,n} = \frac{P_{c,i}}{\dfrac{P_{c,n,s}}{P_{c,n}} + \dfrac{I_n g_c - V_i}{c_n^*(A_c/A_t)}} \qquad (1)$$
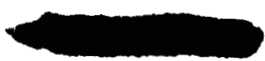
The theoretical value of characteristic velocity at the injector c_i^* can then be computed as follows. Since

$$c_n^* = \frac{P_{c,n} A_t g_c}{\dot{w}}$$

and

$$c_i^* = \frac{P_{c,i} A_t g_c}{\dot{w}}$$

then

$$c_i^* = \frac{P_{c,i}}{P_{c,n}} c_n^* = \left[\frac{P_{c,n,s}}{P_{c,n}} + \frac{I_n g_c - V_i}{c_n^*(A_c/A_t)} \right] c_n^* \qquad (2)$$

Specific impulse. - Ideally, the thrust produced by a rocket engine, assuming one-dimensional flow and expansion to ambient pressure, may be expressed by

$$F = \dot{m} v_e$$

This form is useful for theoretical calculations to keep them general; but, for consideration of practical engines, an additional term λ is required to account for three-dimensional flow through a nozzle having a specified divergence angle:

$$F_d = \dot{m} v_e \lambda = F\lambda$$

Because the exhaust gases from a real engine cannot be expected to expand exactly to the ambient pressure, additional modification is required. Analytically, then, the thrust of a real engine is

$$F_R = F\lambda + (P_e - P_a)A_e$$

Since $I = F/\dot{w}$, the theoretical specific impulse for a real engine is

$$I_R = \frac{F_R}{\dot{w}} = I\lambda + \frac{(P_e - P_a)A_e}{\dot{w}}$$

Theoretical computations, being generalized, do not specify $\dot{w}$ for particular applications, but give values of I and c_n^*. It is therefore convenient to substitute for $\dot{w}$ in terms of c_n^* in the preceding equation:
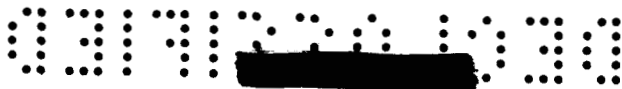
$$I_R = I\lambda + \frac{(P_e - P_a)\frac{A_e}{A_t} c_n^*}{P_{c,n} g_c} \tag{3}$$

In practice, to compute I_R for specific engine and operational conditions, the terms are obtained as follows: λ, A_e, A_t, and P_a are determined from measurements; I, c_n^*, and P_e come from theoretical data pertinent to the $P_{c,n}$, A_e/A_t, and propellant mixture ratio of the operation; $P_{c,n}$ is calculated from the measured $P_{c,i}$ by equation (1).

Nozzle thrust coefficient. - Values of nozzle thrust coefficient are determined simply by the equation

$$C_{F,R} = \frac{I_R g_c}{c_i^*} \tag{4}$$

REFERENCES

1. Gordon, Sanford, and Huff, Vearl N.: Theoretical Performance of Liquid Hydrogen and Liquid Fluorine as a Rocket Propellant. NACA RM E52L11, 1953.

2. Curren, Arthur N., Price, Harold G., Jr., and Douglass, Howard W.: Analysis of Effects of Rocket-Engine Design Parameters on the Regenerative Cooling Capabilities of Several Propellants. NASA TN D-66, 1959.

3. Rothenberg, Edward A., Kutina, Franklin J., Jr., and Kinney, George R.: Experimental Performance of Gaseous Hydrogen and Liquid Oxygen in Uncooled 20,000-Pound-Thrust Rocket Engines. NASA MEMO 4-8-59E, 1959.

4. Heidmann, M. F., and Baker, Louis, Jr.: Combustor Performance with Various Hydrogen-Oxygen Injection Methods in a 200-Pound-Thrust Rocket Engine. NACA RM E58E21, 1958.

5. Auble, Carmon M.: A Study of Injection Processes for Liquid Oxygen and Gaseous Hydrogen in a 200-Pound-Thrust Rocket Engine. NACA RM E56I25a, 1957.

6. Otto, Edward W., and Flage, Richard A.: Control of Combustion-Chamber Pressure and Oxidant-Fuel Ratio for a Regeneratively Cooled Hydrogen-Fluorine Rocket Engine. NASA TN D-82, 1959.

7. Schmidt, Harold W.: Reaction of Fluorine with Carbon as a Means of Fluorine Disposal. NACA RM E57E02, 1957.

8. Huff, Vearl N., Fortini, Anthony, and Gordon, Sanford: Theoretical Performance of JP-4 Fuel and Liquid Oxygen as a Rocket Propellant. II - Equilibrium Composition. NACA RM E56D23, 1956.

E-183

TABLE I. - ENGINE GEOMETRY
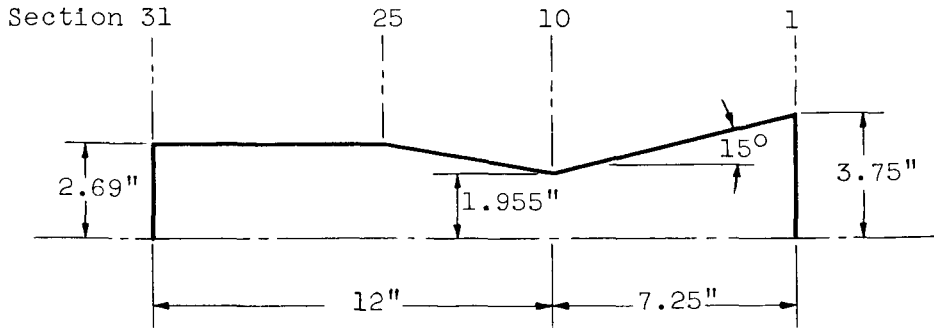
Section	Local engine diameter, in.	Coolant-passage height, in.		Length of coolant passage between sections, in.
		Engine 1	Engine 2	
1	7.5	0.203	0.230	0
2	6.98	.186	.209	1.00
3	6.49	.169	.188	1.00
4	5.96	.152	.168	1.00
5	5.44	.135	.147	1.00
6	4.94	.119	.126	1.00
7	4.43	.100	.105	1.00
8	4.16	.090	.096	.53
9	3.98	.082	.085	.49
10	3.91	.076	.078	.40
11	3.92	.082	.080	.28
12	3.98	.087	.082	.27
13	4.08	.091	.084	.32
14	4.20	.092	.086	.22
15	4.30	.091	.088	.27
16	4.51	.082	.090	.50
17	4.70	.082	.093	.50
18	4.85	.084	.097	.50
19	4.99	.087	.099	.50
20	5.10	.090	.100	.50
21	5.20	.092	.101	.50
22	5.27	.095	.101	.50
23	5.32	.097	.101	.50
24	5.36	.099	.099	.50
25	5.38	.100	.098	.50
26	5.38	.100	.096	1.00
27	5.38	.100	.092	1.00
28	5.38	.100	.092	1.00
29	5.38	.100	.089	1.00
30	5.38	.100	.086	1.00
31	5.38	.100	.084	.82

DECLASSIFIED

TABLE II. – PERFORMANCE OF LIQUID HYDROGEN AND LIQUID FLUORINE IN REGENERATIVELY COOLED ROCKET ENGINES

Engine	Injector type	Experimental values								Theoretical values									Experimental efficiency							
		Fuel, weight percent	Propellant total flow rate, lb/sec	Thrust, lb	Combustion pressure, $P_{c,1}$, lb/sq in. abs	Specific impulse, I_x, lb-sec/lb	Specific impulse corrected to vacuum conditions, $I_{,vac}$, lb-sec/lb	Characteristic velocity, c_x^*, ft/sec	Nozzle thrust coefficient, $C_{F,x}$	Ideal specific impulse, I_{id}, lb-sec/lb Equilibrium	Frozen	Real specific impulse, I_R, lb-sec/lb Equilibrium	Frozen	Characteristic velocity, c^*, ft/sec Equilibrium	Frozen	Nozzle thrust coefficient, $C_{F,R}=\frac{I_R g}{c^*}$ Equilibrium	Frozen	$\frac{I_x}{I_{id}}$ Equilibrium	Frozen	$\frac{I_x}{I_R}$ Equilibrium	Frozen	$\frac{c_x^*}{c_R^*}$ Equilibrium	Frozen	$\frac{C_{F,x}}{C_{F,R}}$ Equilibrium	Frozen
1	Shower-head	18.97	17.20	6050	382	351.7	388.8	8689	1.302	361.8	355.0	364.1	358.2	8773	8647	1.335	1.333	0.972	0.991	0.966	0.982	0.990	1.005	0.975	0.977
		19.63	14.07	4865	302	345.9	390.9	8385	1.327	361.0	355.3	353.6	348.3	8749	8631	1.300	1.298	.958	.974	.978	.993	.958	.972	1.021	1.022
		15.78	13.90	4870	302	350.2	395.2	8483	1.328	364.4	352.5	357.2	345.3	8771	8565	1.310	1.297	.961	.993	.980	1.014	.967	.990	1.014	1.024
		11.66	14.01	4874	301	347.9	393.1	8415	1.330	362.7	344.1	355.7	336.5	8648	8387	1.323	1.291	.959	1.011	.978	1.034	.973	1.003	1.005	1.050
		10.80	15.00	5201	322	346.7	388.5	8394	1.329	361.4	341.9	357.9	337.6	8597	8333	1.339	1.303	.959	1.014	.969	1.027	.976	1.007	.993	1.020
		8.95	15.21	5201	321	342.0	383.5	8255	1.333	358.0	336.4	354.5	332.0	8503	8219	1.341	1.299	.955	1.017	.965	1.030	.971	1.004	.994	1.026
		7.02	15.85	5158	319	325.4	365.2	7875	1.329	353.5	329.0	349.8	324.3	8380	8061	1.343	1.294	.921	.989	.930	1.003	.940	.977	.990	1.027
2	Triplet	13.79	14.24	5013	312	351.9	396.7	8472	1.336	364.5	349.2	359.3	343.5	8718	8483	1.315	1.303	0.965	1.008	0.979	1.024	0.972	0.999	1.016	1.025
		9.78	14.75	5047	313	342.6	385.9	8208	1.343	359.6	339.0	355.0	333.2	8541	8264	1.337	1.297	.953	1.011	.965	1.028	.961	.993	1.004	1.035
		7.96	14.96	4952	310	331.0	373.6	7993	1.332	356.0	333.0	350.6	326.8	8457	8132	1.334	1.293	.930	.994	.944	1.013	.945	.983	.999	1.030
		6.12	16.06	5040	311	313.8	353.5	7488	1.348	350.4	323.7	345.7	317.6	8277	7933	1.344	1.288	.896	.969	.908	.988	.905	.944	1.003	1.047

[a] Based on chamber pressure measured at injector face.

TABLE III. – HEAT-TRANSFER RESULTS

Fuel, weight percent	Experimental							Analytical Coolant inlet temperature, °R 100 Per-cent	$\frac{c_p^* t}{c_p^* t}\times 100$ Experimental efficiency	Coolant outlet temperature, °R 100 Per-cent	Experimental efficiency	Heat flux, Btu/(sq in.)(sec) Exit 100 Per-cent	Exit Experimental efficiency	Throat 100 Per-cent	Throat Experimental efficiency	Chamber 100 Per-cent	Chamber Experimental efficiency	Average heat flux, Btu/(sq in.)(sec) 100 Per-cent	Experimental efficiency	Gas-side wall temperature, °R Exit 100 Per-cent	Exit Experimental efficiency	Throat 100 Per-cent	Throat Experimental efficiency	Chamber 100 Per-cent	Chamber Experimental efficiency	Minimum coolant density, lb/cu ft 100 Per-cent	Experimental efficiency	Maximum coolant velocity, ft/sec 100 Per-cent	Experimental efficiency	Engine coolant ΔP, lb/sq in. 100 Per-cent	Experimental efficiency
	Average coolant outlet temperature, °R	Average coolant inlet temperature, °R	Average coolant density, lb/cu ft	Coolant flow rate, lb/sec	Average heat flux, Btu/(sq in.)(sec)	Engine coolant ΔP, lb/sq in.	Injector hydrogen ΔP, lb/sq in.																								
18.97	195	46.3	0.428	3.263	4.90	129	65	50	50	265	274	2.76	2.98	11.60	11.12	6.74	6.43	620	600	796	745	934	945	0.177	0.186	1589	1467	141	145
19.63	201	45.8	.314	2.762	4.55	90	38			270	296	2.73	2.63	11.52	11.08	6.70	6.40	600	727	772	722	960	920	.177	.161	1640	1350	133	123
15.78	272	45.8	.255	2.194	5.29	81	36			334	318	2.45	2.36	11.50	11.40	6.90	6.61	860	757	921	987	1091	998	.171	.171	1295	1252	115	113
11.66	450	46.1	.100	1.633	5.49	83	28			448	412	2.85	2.98	10.99	10.50	7.58	7.41	945	945	1067	1194	1374	1260	.143	.157	1160	1090	78	76
10.80	530	61.0	.135	1.620	6.47	85	23			614	443	3.35	3.49	13.80	12.90	7.85	7.78	1009	1148	1270	1409	1339	1150	.154	.149	1190	1150	72	72
8.95	624	56.2	.108	1.561	7.26	70	17			870	606	3.02	2.88	16.20	16.00	7.34	7.18	1148	1231	1520	1735	1585	1590	.103	.128	1185	1045	60	56
7.02	563	54.6	.090	1.113	7.09	72	79			370	355	2.91	2.94	11.69	11.40	6.78	6.62	845	845	1040	1190	1000	941	.100	.117	1307	1045	49	49
13.79	553	46.0	.120	1.984	6.92	138	65			540	483	2.31	2.31	13.00	13.00	6.78	6.35	965	965	1040	1160	1240	1160	.123	.134	1415	1350	88	88
9.78	688	46.0	.120	1.440	7.64	110	51			735	483	2.68	3.02	14.90	14.90	7.20	7.00	1160	1160	1240	1400	1590	1530	.121	.137	1490	1450	69	69
7.96	553	46.0	.101	1.191	8.50	96	22			735	589	2.92	3.05	15.98	15.98	7.12	6.60	1200	1392	1620	2045	1590	1429	.092	.118	1590	1212	59	51
6.12	710	46.0	.080	.984	7.25	68	22			1010	635	3.23	3.25	16.90	10.38	4.07	6.52	1100	1735	2490	2870	1560	1560	.068	.119	1690	990	35	35

[a] Maximum coolant density, at inlet, was considered to be 4.360 lb/cu ft at 40° R.

Figure 1. - Two types of hydrogen-fluorine injectors for 5000-pound-thrust rocket.

E-183

CK-4 back

CD-6708

Figure 2. - Fuel-cooling of injector.

Face plate

Fuel

Distribution plate

Oxidant

C-46610

E-183

Figure 3. - Assembly of hydrogen-fluorine thrust chamber.

E-183

Cross section of
single channel

Stainless-steel wire

72 Longitudinal
nickel channels

Completed engine

0 INCH 1

CS-15324
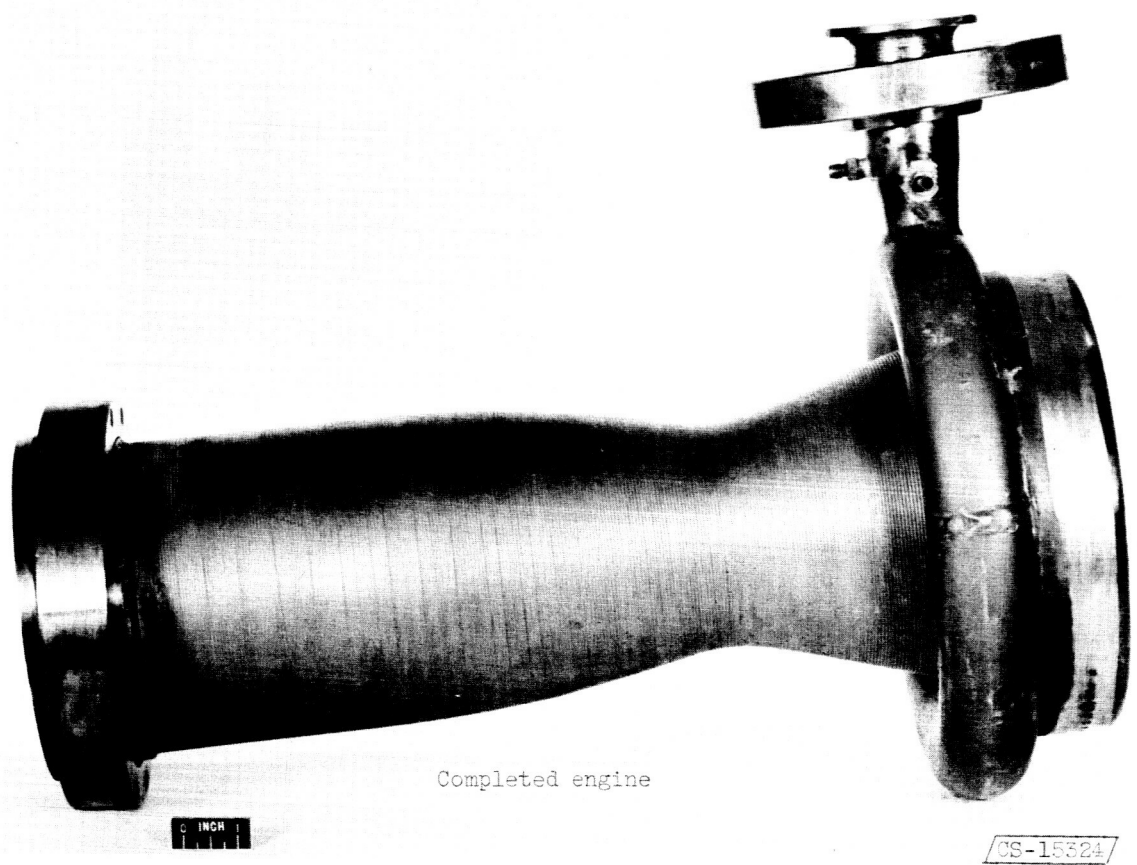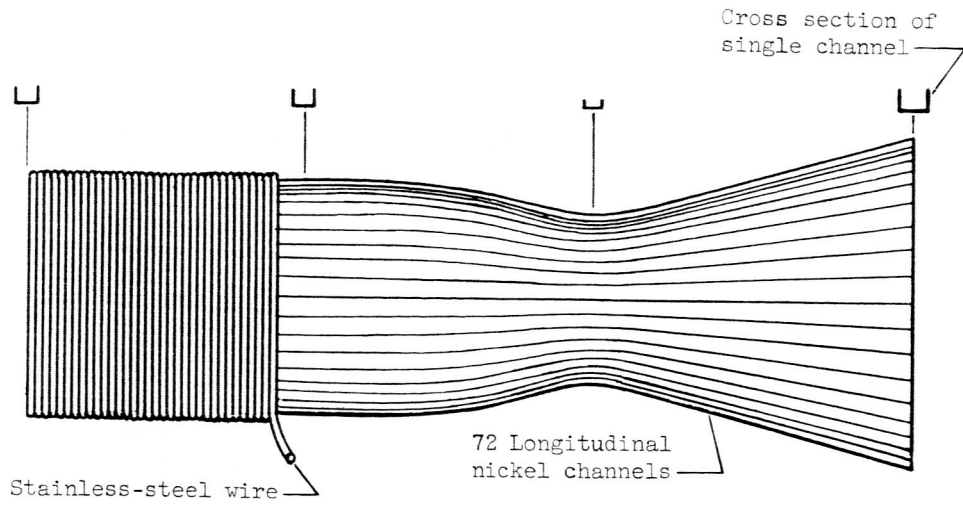
Figure 4. - Detail of thrust chamber.
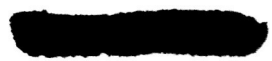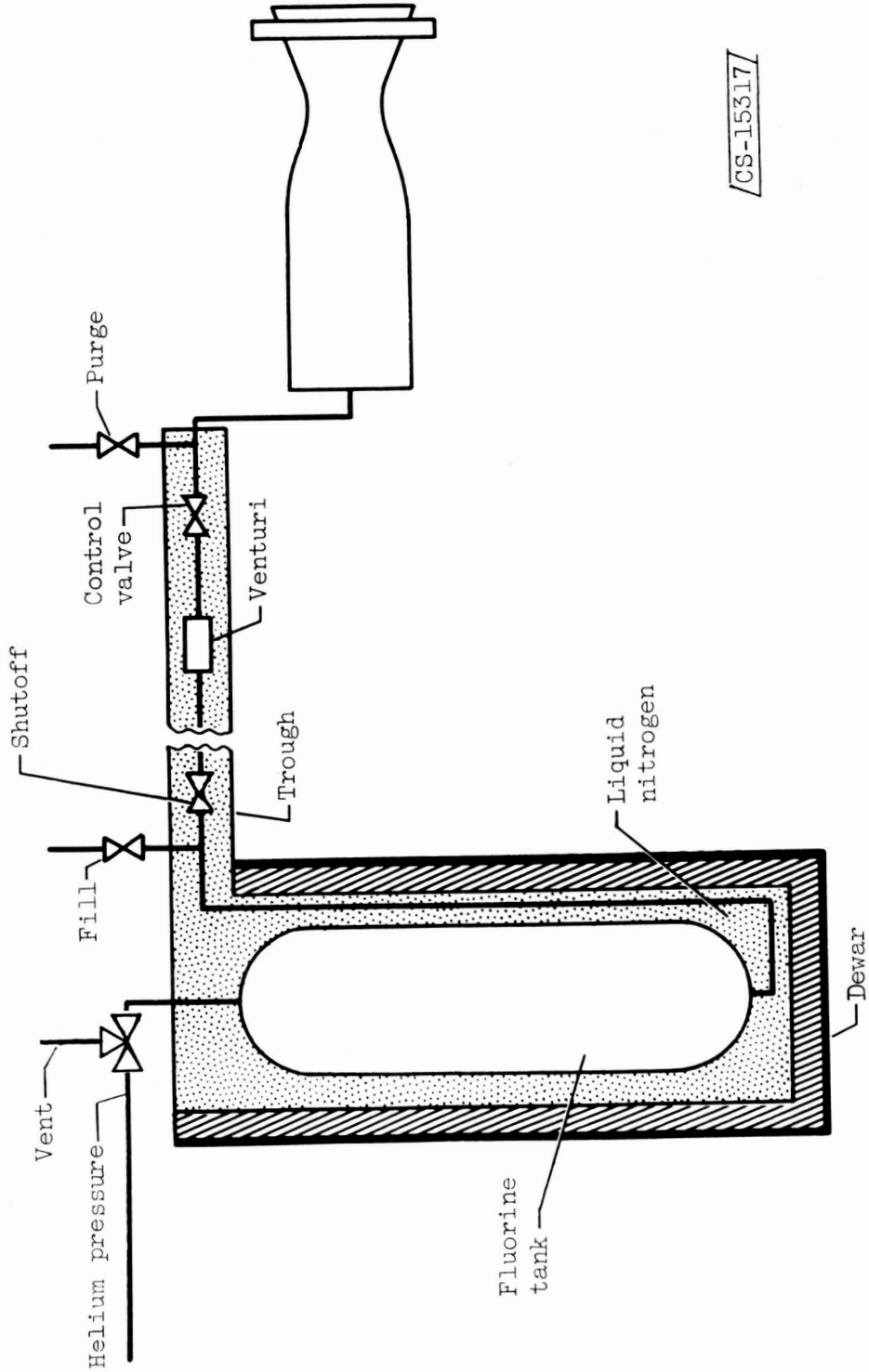
Figure 5. - Fluorine flow system.

CS-15317
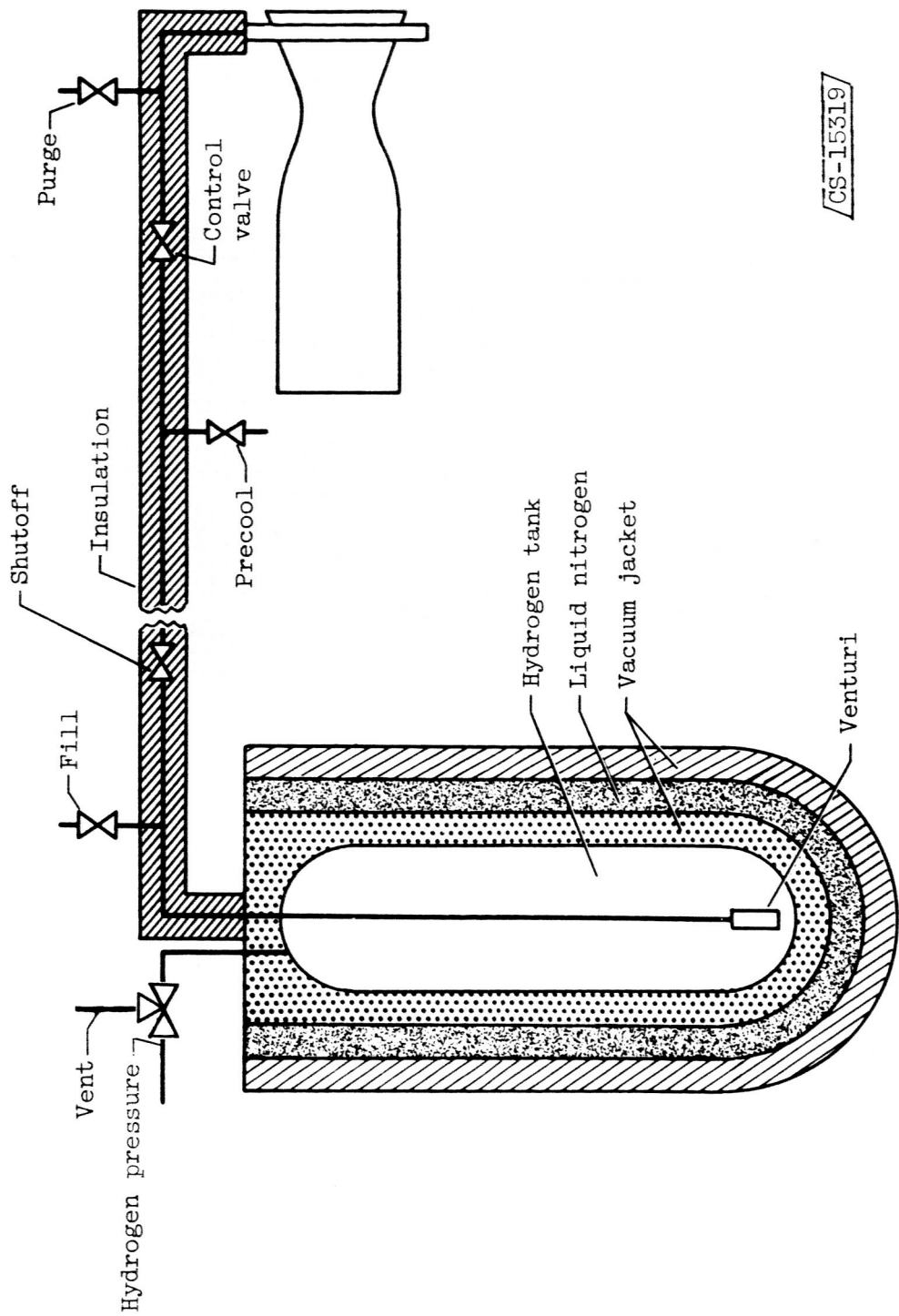
E-183

Figure 6. - Hydrogen flow system.

CS-15319

C-47324

(a) Photograph.

Water spray bars

Test-cell wall

Carbon dioxide spray bar

Water jet wheel

Rocket engine

Carbon dioxide
spray bar

Sump

CS-15320

Water
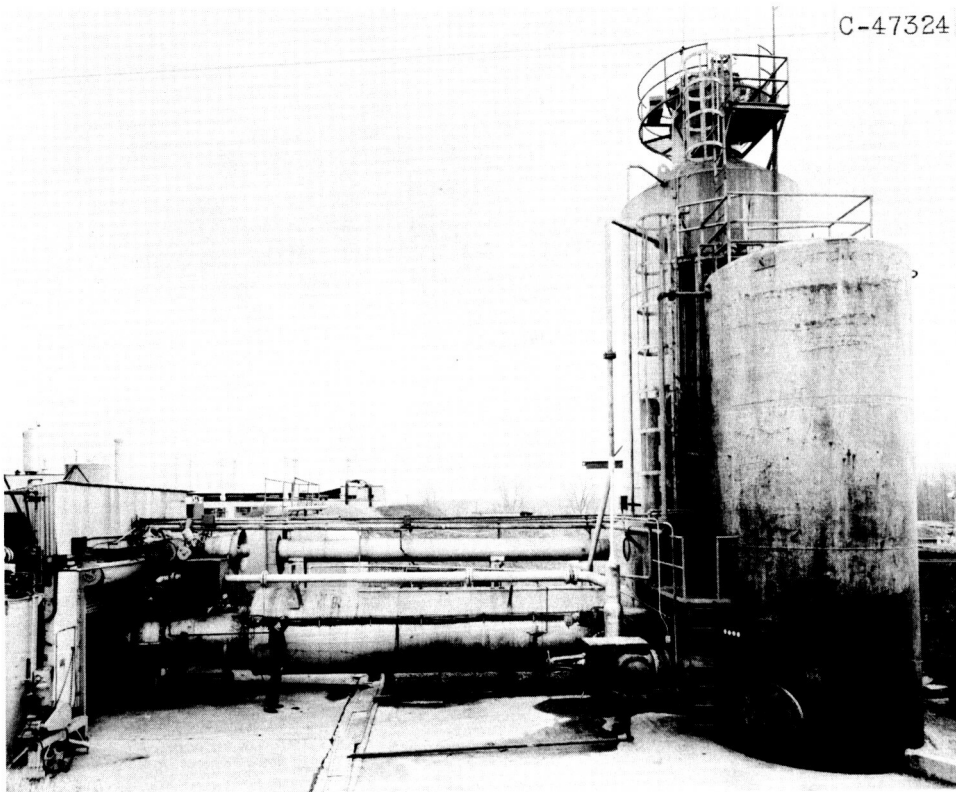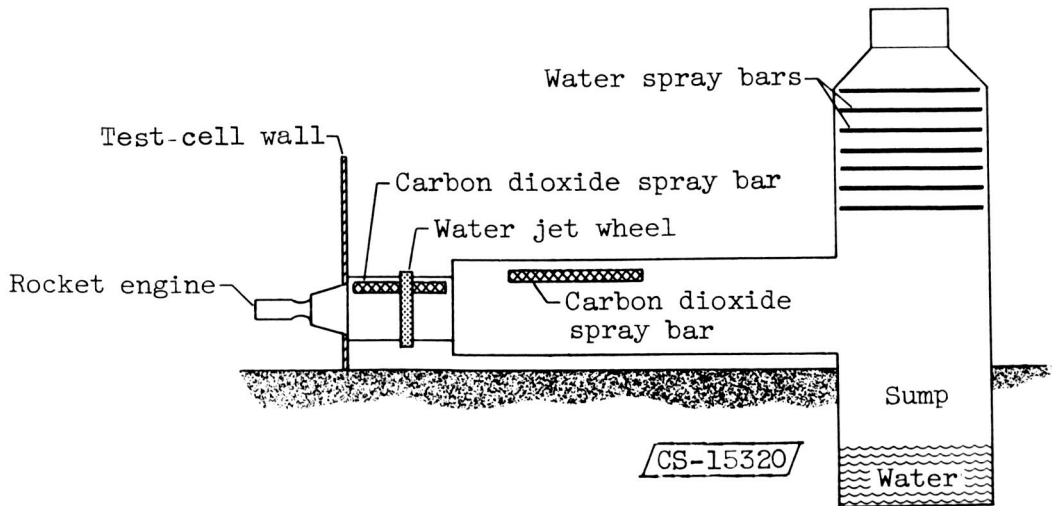
(b) Schematic diagram.

Figure 7. - Rocket exhaust-gas scrubber.

E-183

CK-5

C-46775

Thrust chamber

Floating bed

Structural frame

Flexure plate
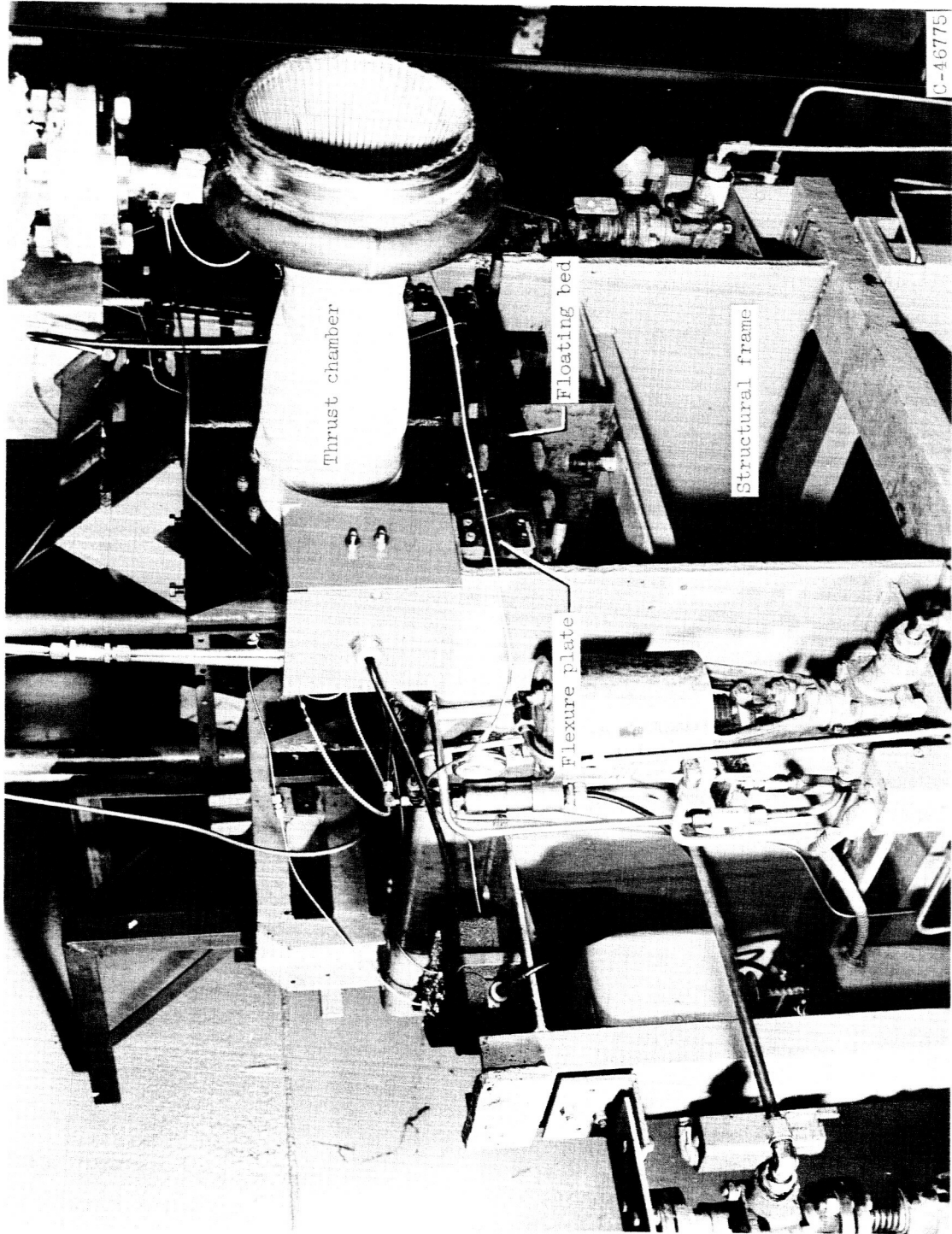
Figure 8. - Thrust chamber mounted on stand.

E-183

Position-indicator housing

Hydraulic actuator

Packing gland and yoke

Pressurized-bellows-seal enclosure

Commercial valve body
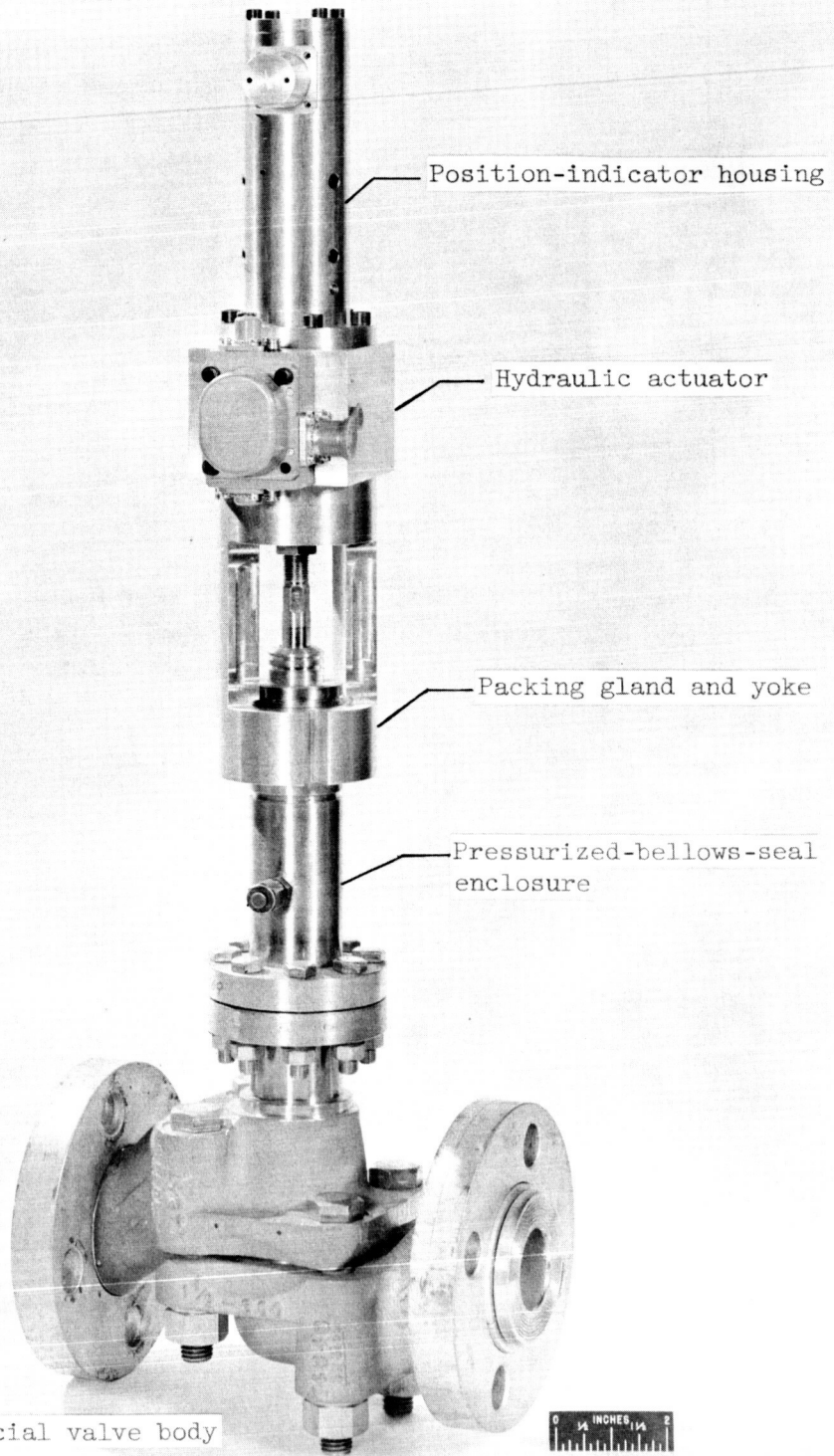
C-49994

Figure 9. - Automatic servo-operated flow control valve.

E-183

CX-5 back
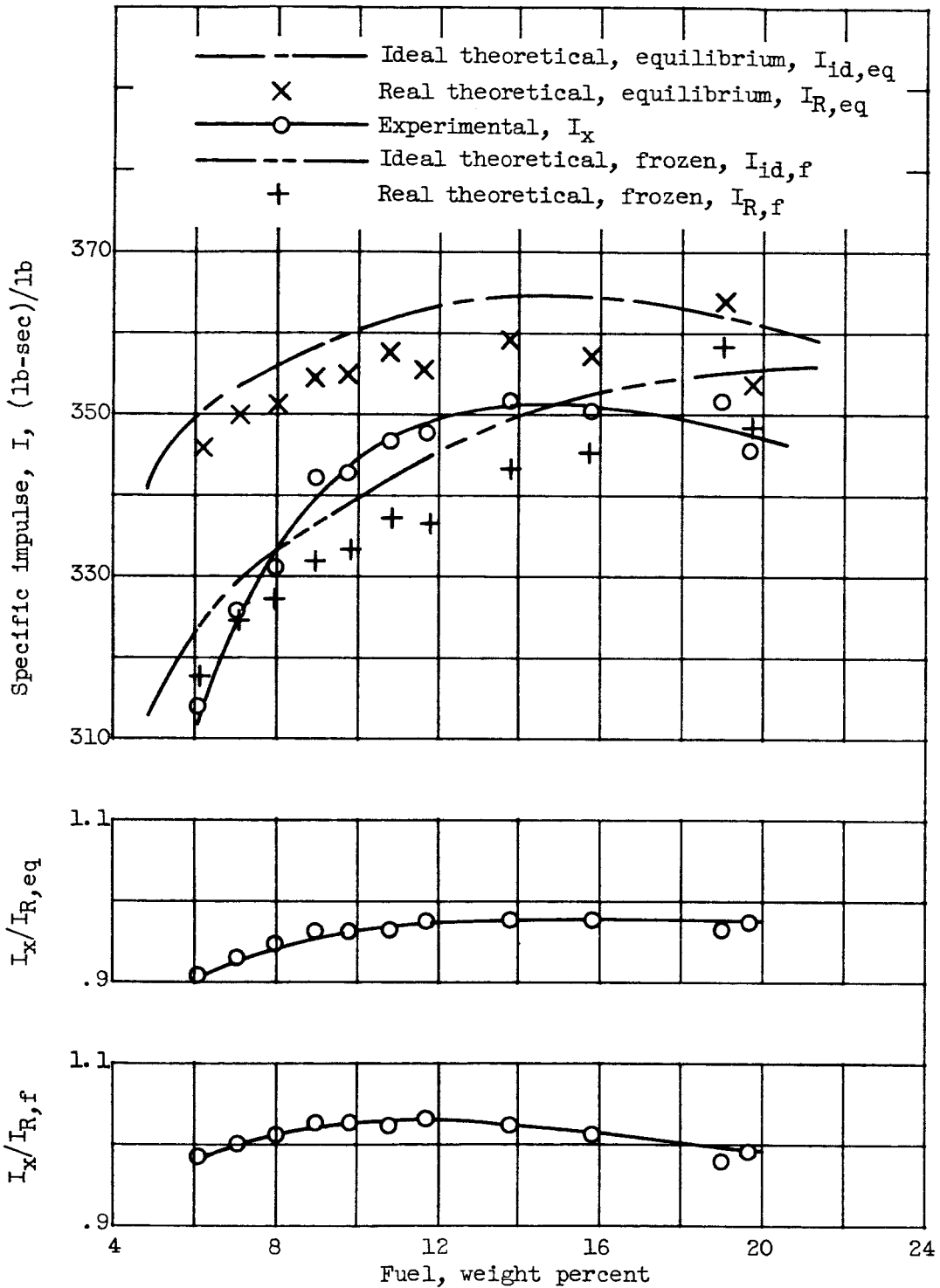
(a) Specific impulse.

Figure 10. - Experimental performance of hydrogen-fluorine.
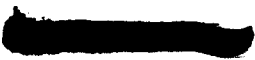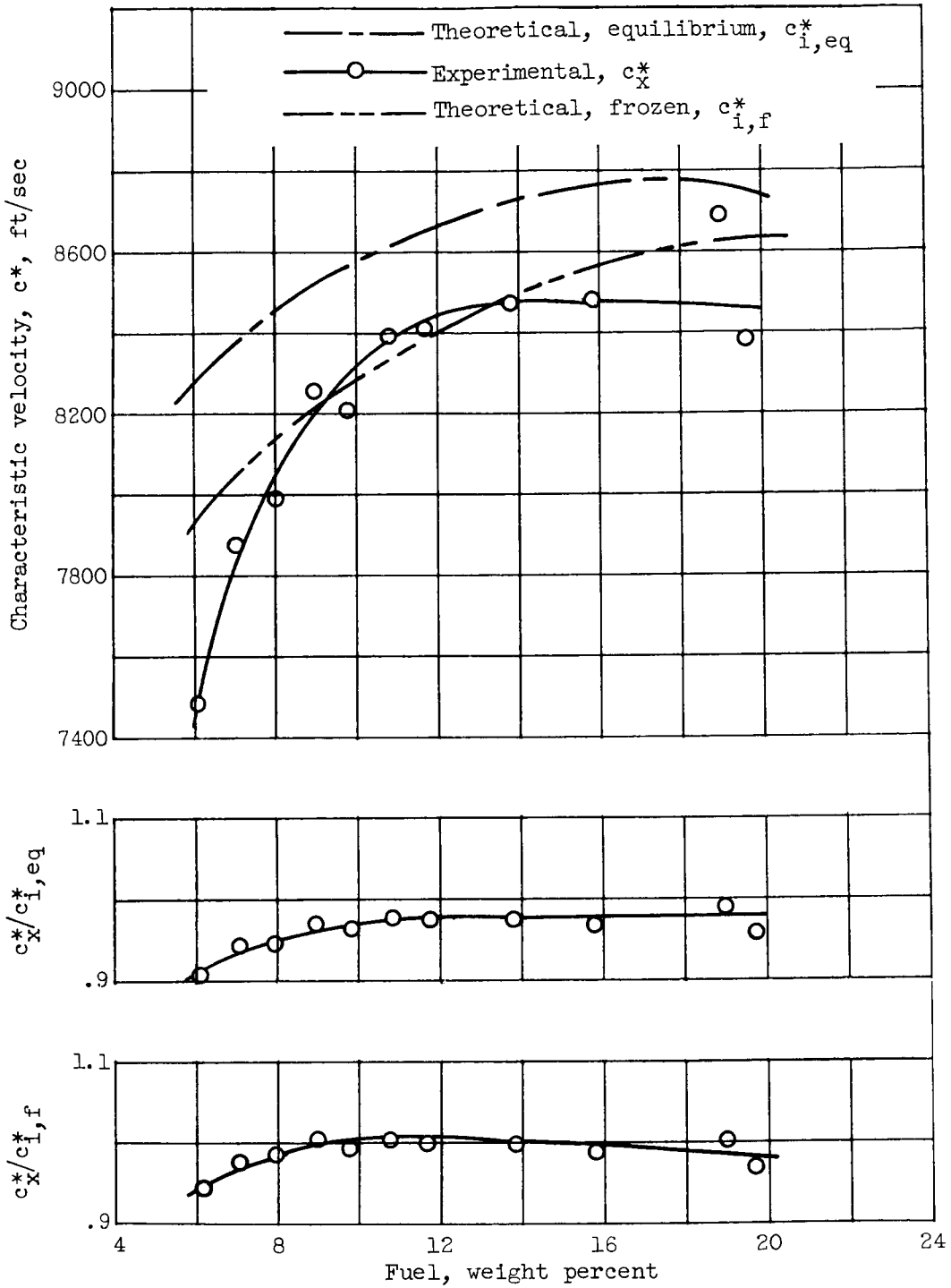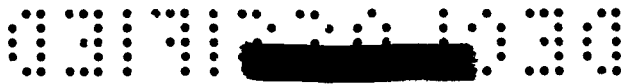
(b) Characteristic velocity.

Figure 10. - Continued.   Experimental performance of
hydrogen-fluorine.

E-183
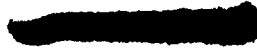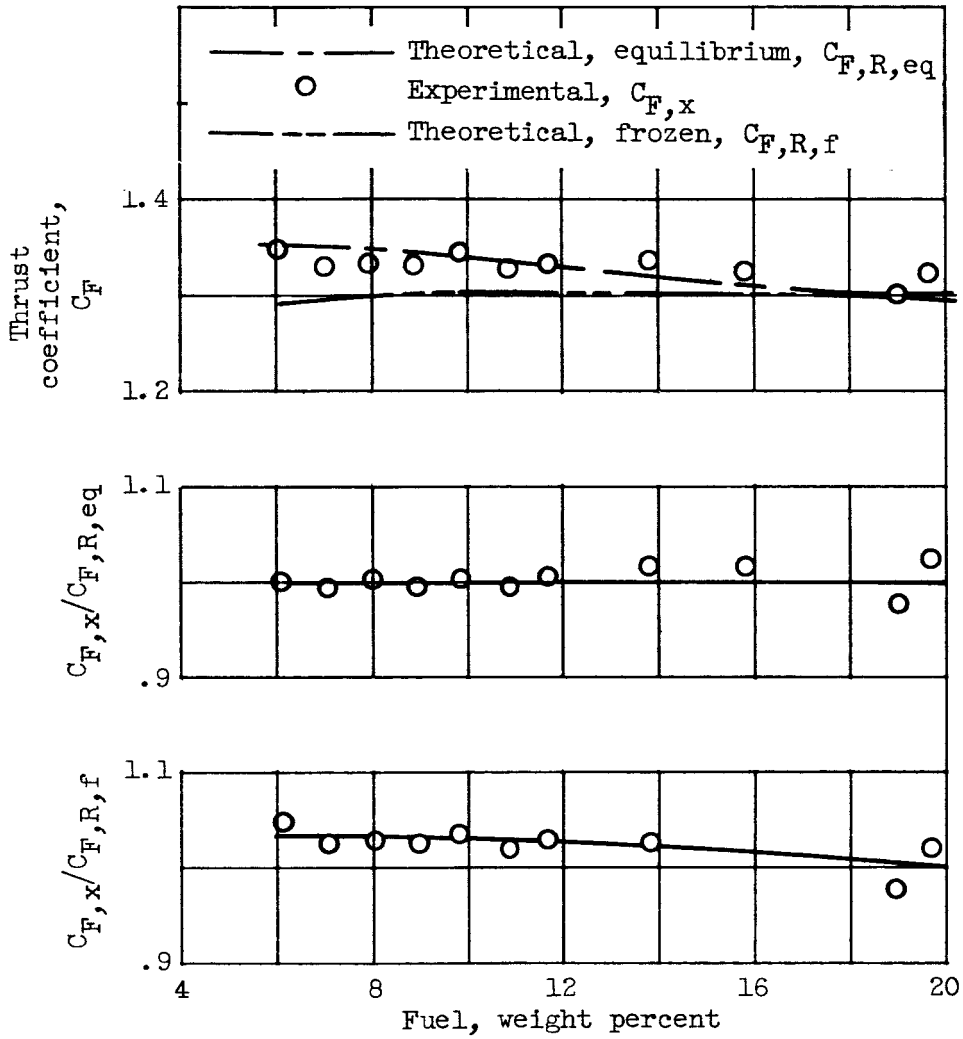
(c) Nozzle thrust coefficient.

Figure 10. - Concluded. Experimental performance
of hydrogen-fluorine.
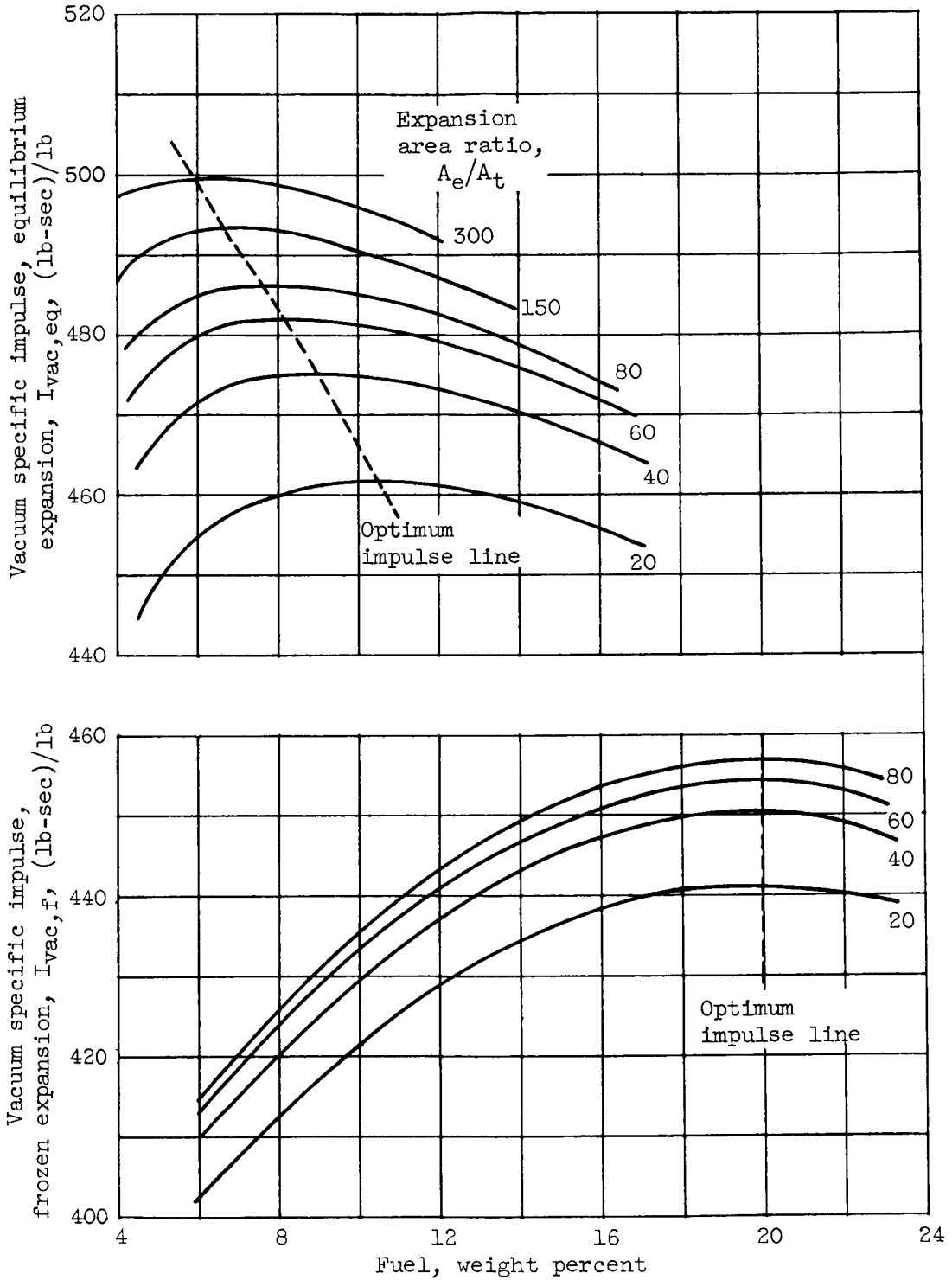
Figure 11. - Theoretical vacuum specific impulse for hydrogen-
fluorine at chamber pressure of 300 pounds per square inch
absolute as function of expansion area ratio.
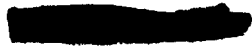
E-183

E-183
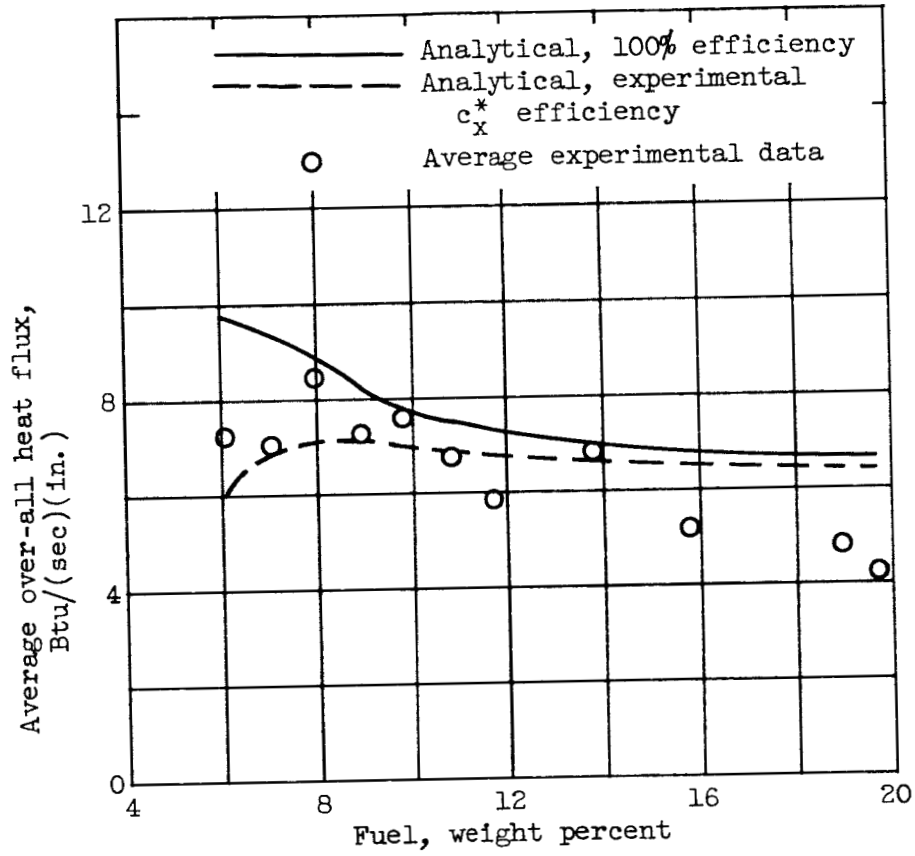
Figure 12. - Average over-all heat flux with
hydrogen-fluorine.
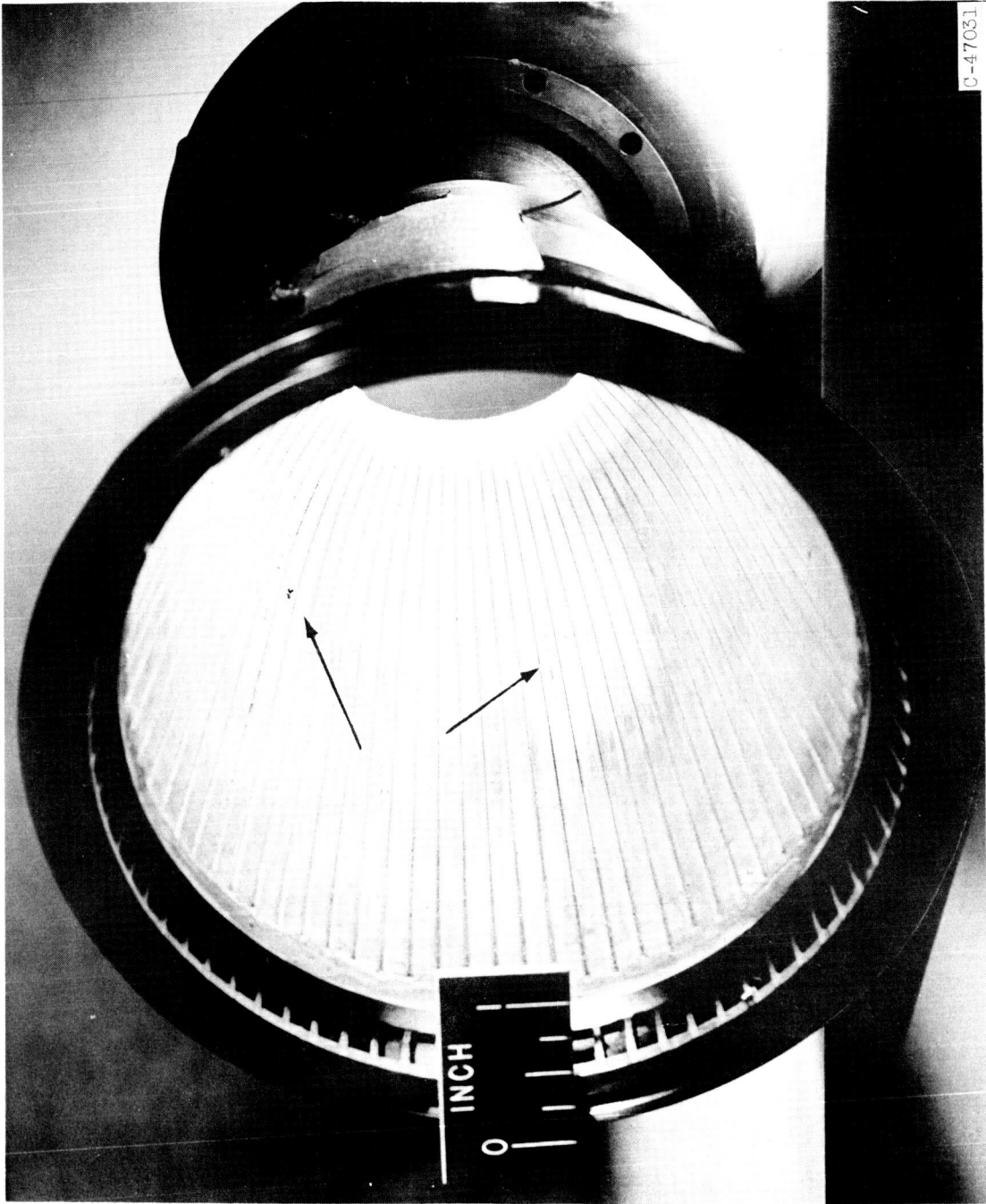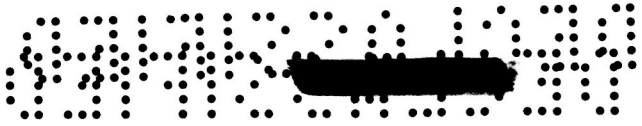
Figure 13. - Areas of slight burning of combustion-chamber walls. Locations of burned holes can be related to injector pattern.

E-183

C-47395

E-183

CK-6
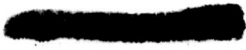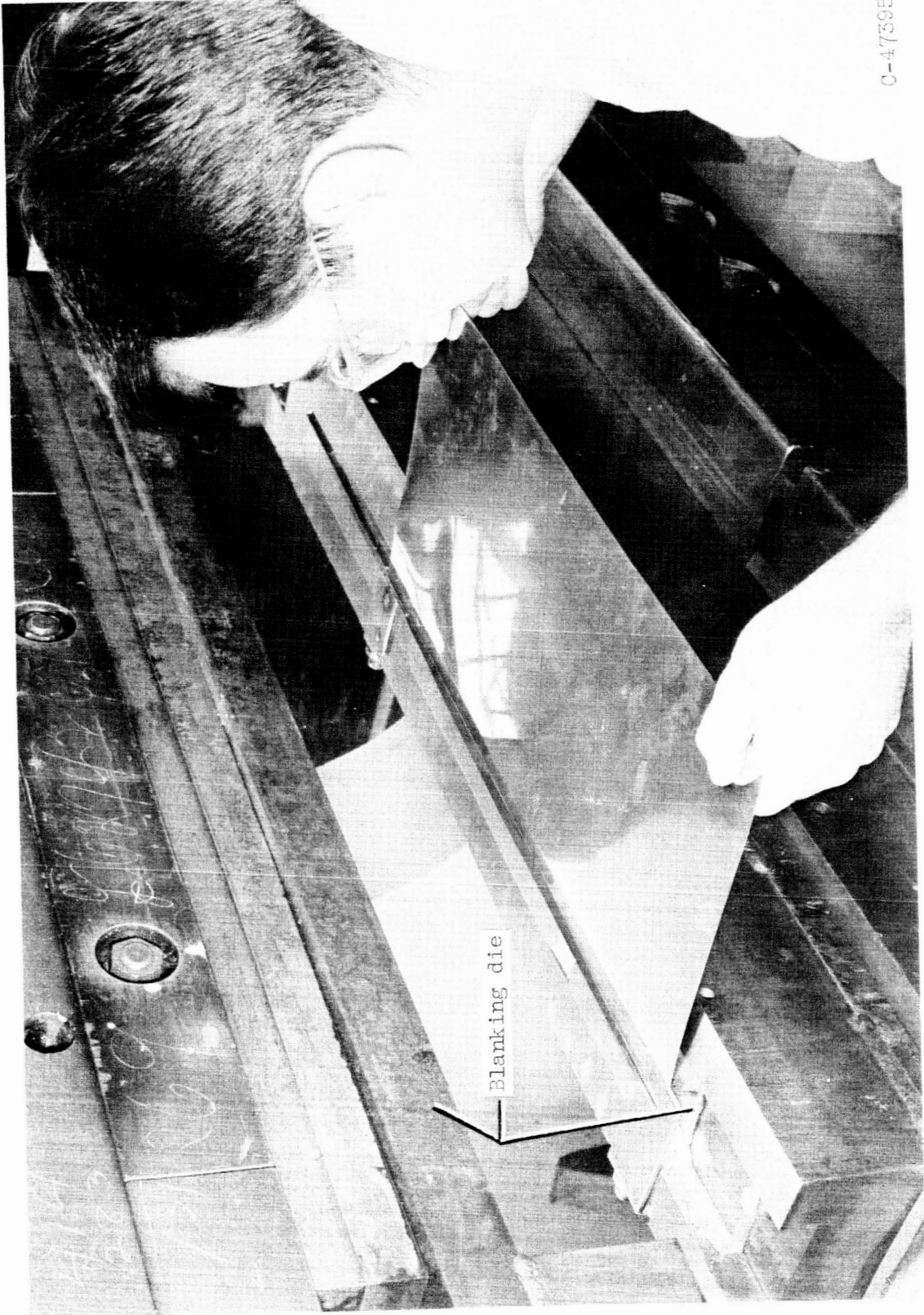
Blanking die

Figure 14. - Blanking operation.
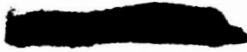
C-47402

Figure 15. - Removing formed channel from die.

E-183

CK-6 'back '

C-47937

Three-piece female forming die.

Die holder

Shim

Hydraulic pressure cell
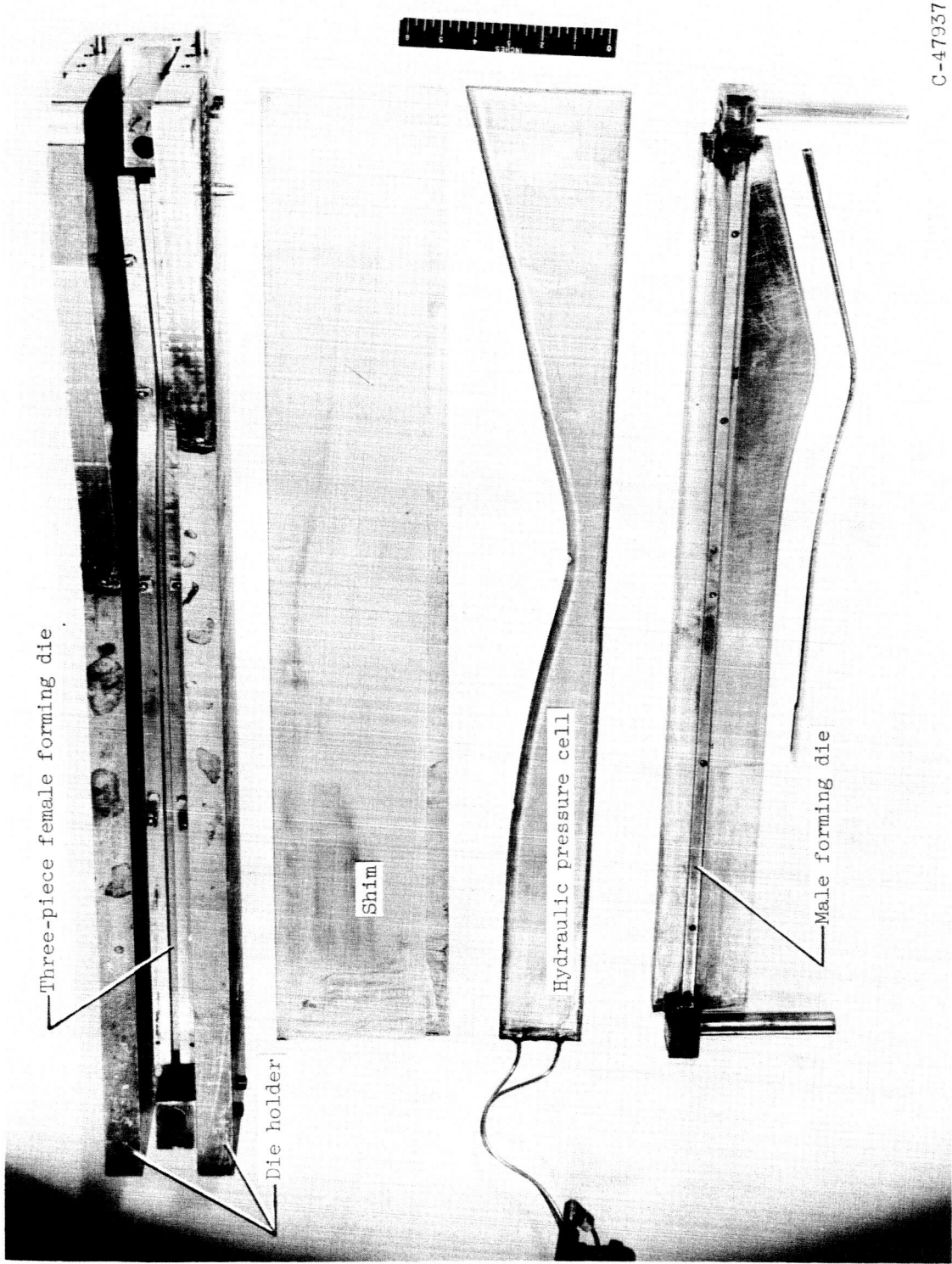
Male forming die

Figure 16. - Components of forming die.
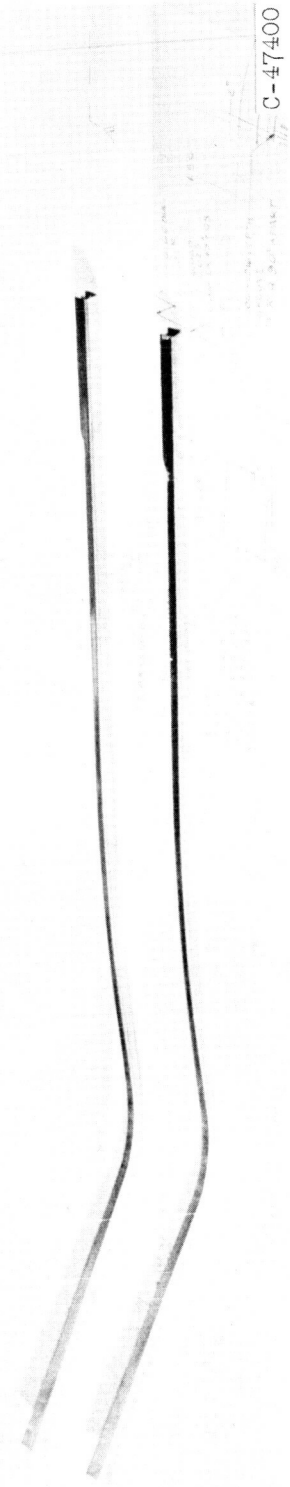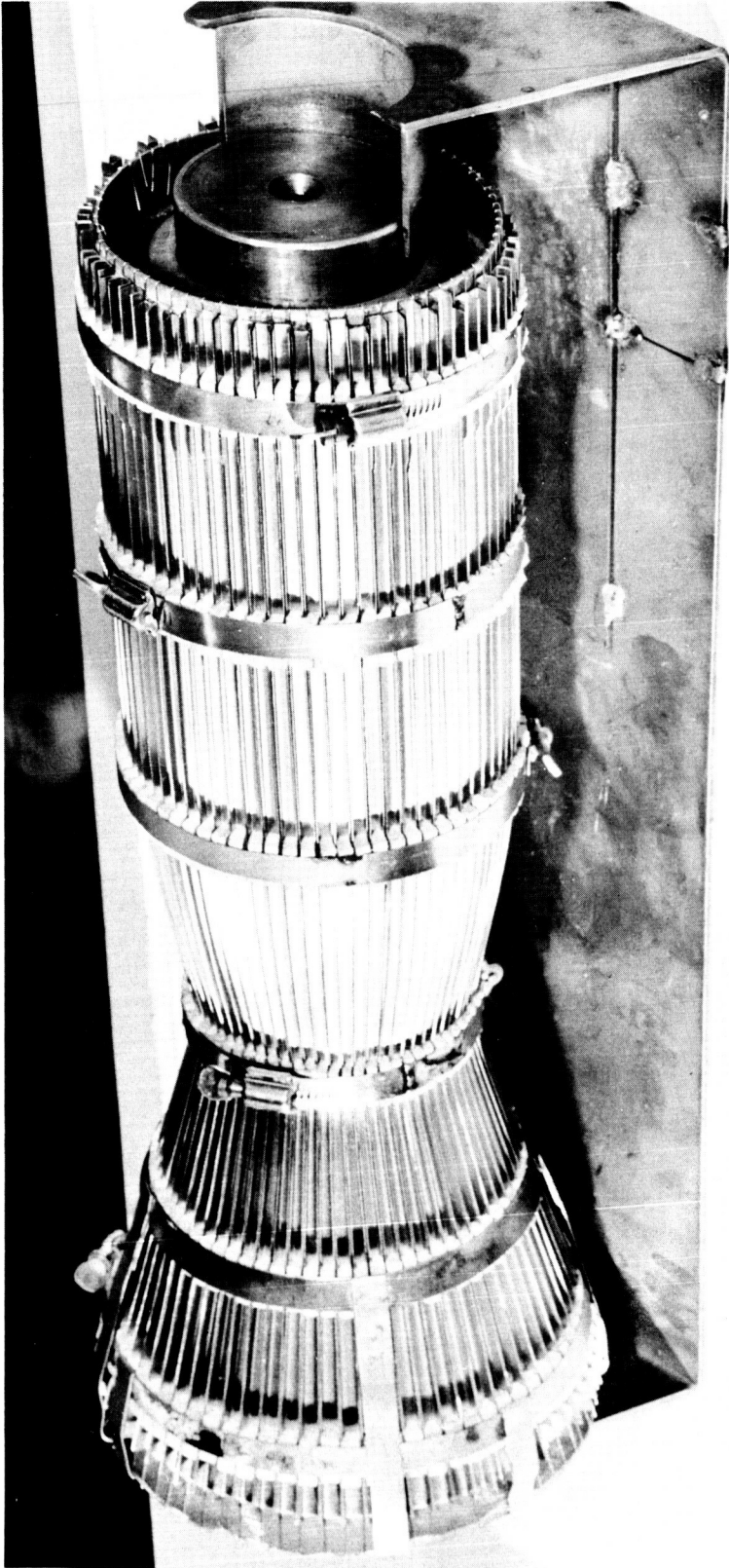
Figure 17. - Bundled channel assembly.

E-183

C-47400

E-183

C-47401

Figure 18. - Spot-welding channels with standard spot-welding machine.
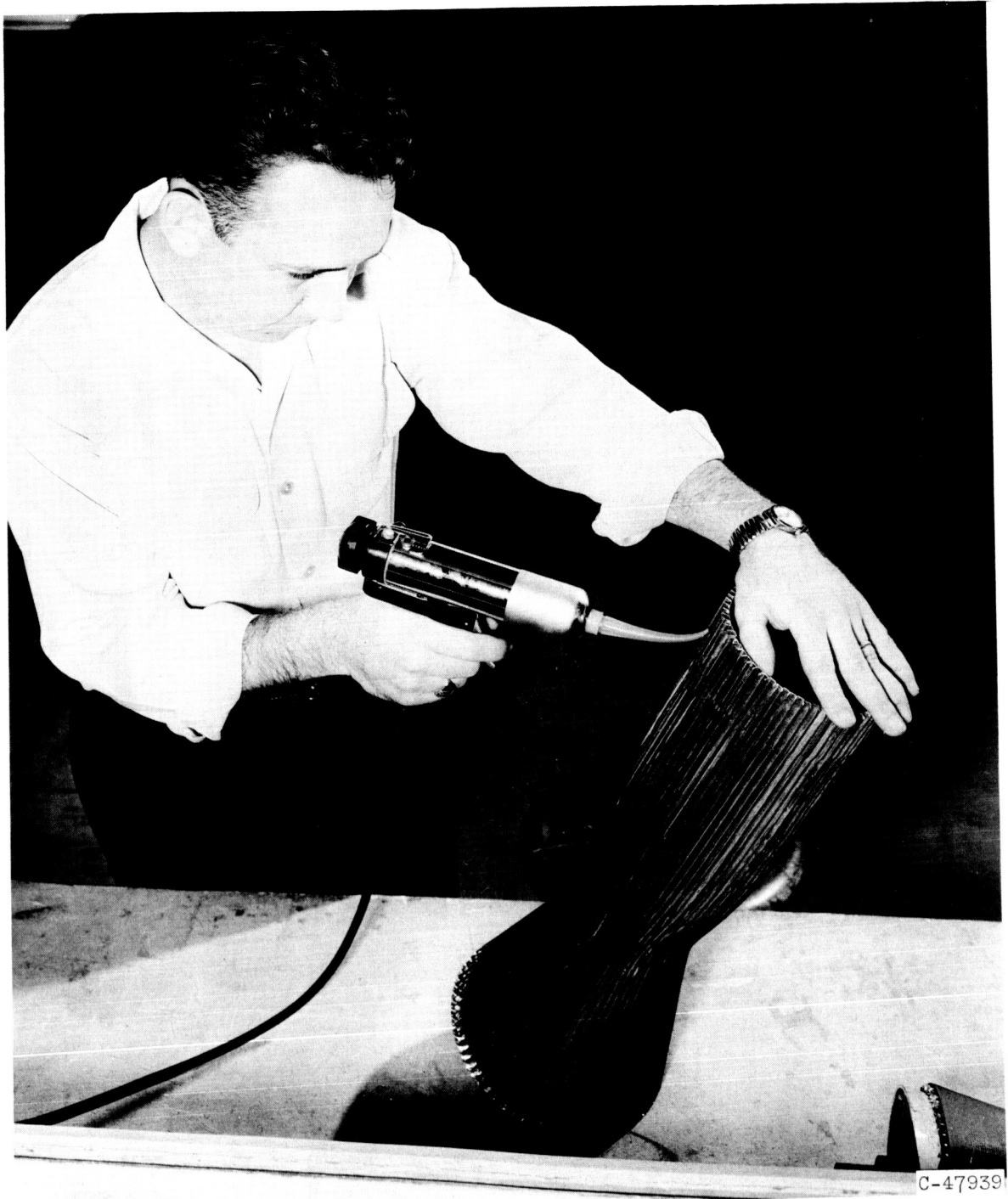
Figure 19. - Applying braze alloy to channels.
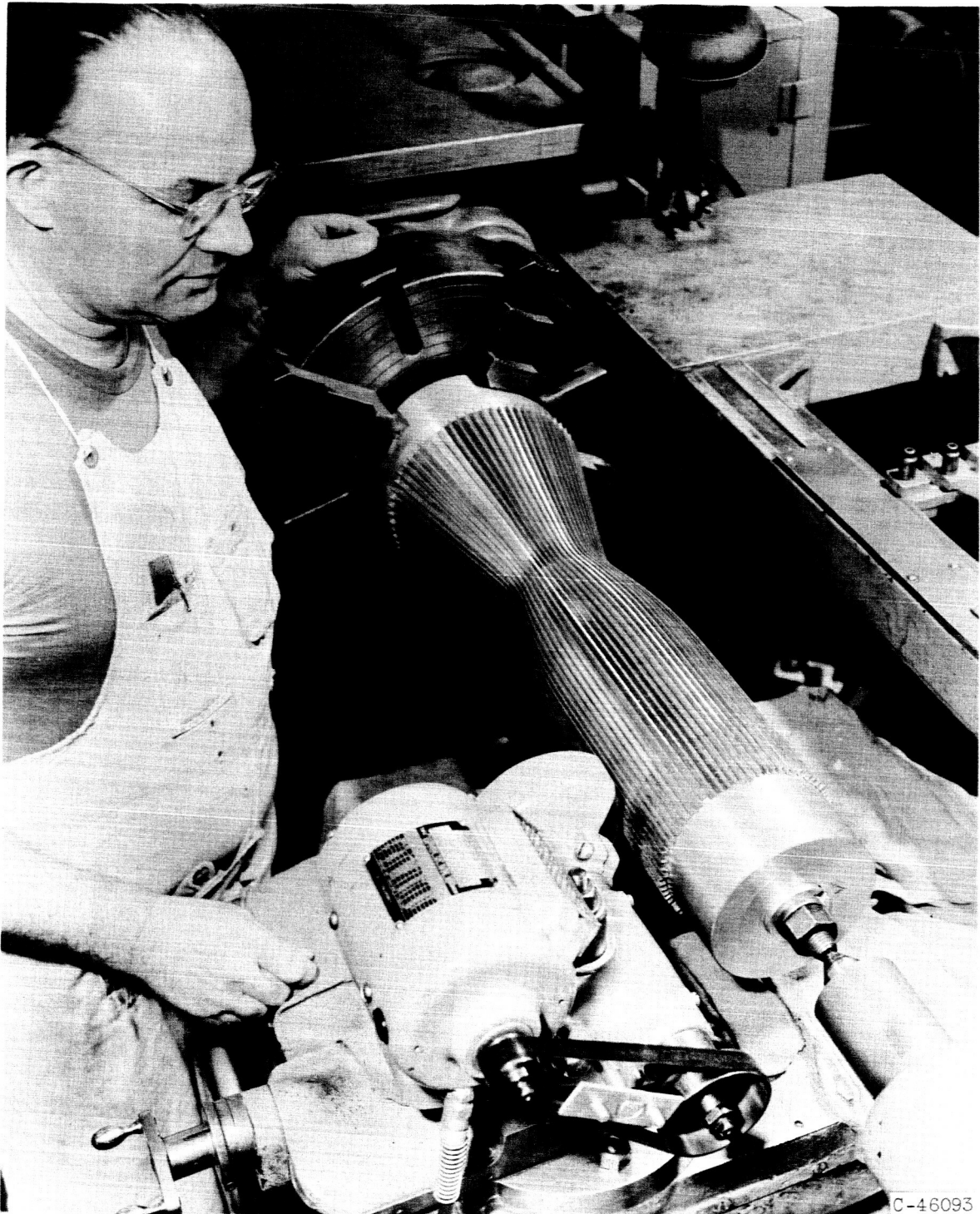
C-47939

E-183

E-183

Figure 20. - Dry-grinding channels to desired contour.

C-46093
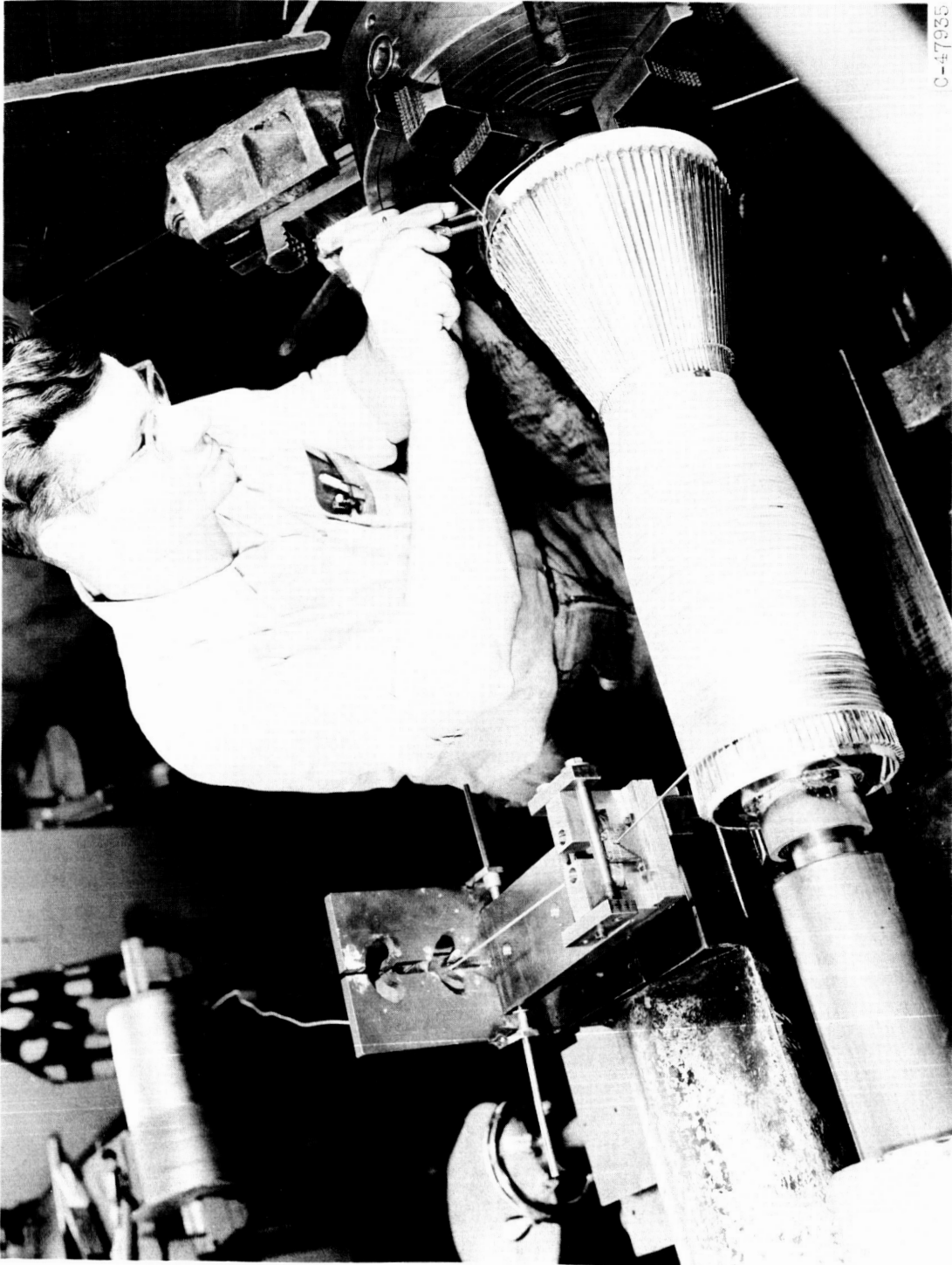
E-183

Figure 21. - Wire-wrapping of channel assembly.
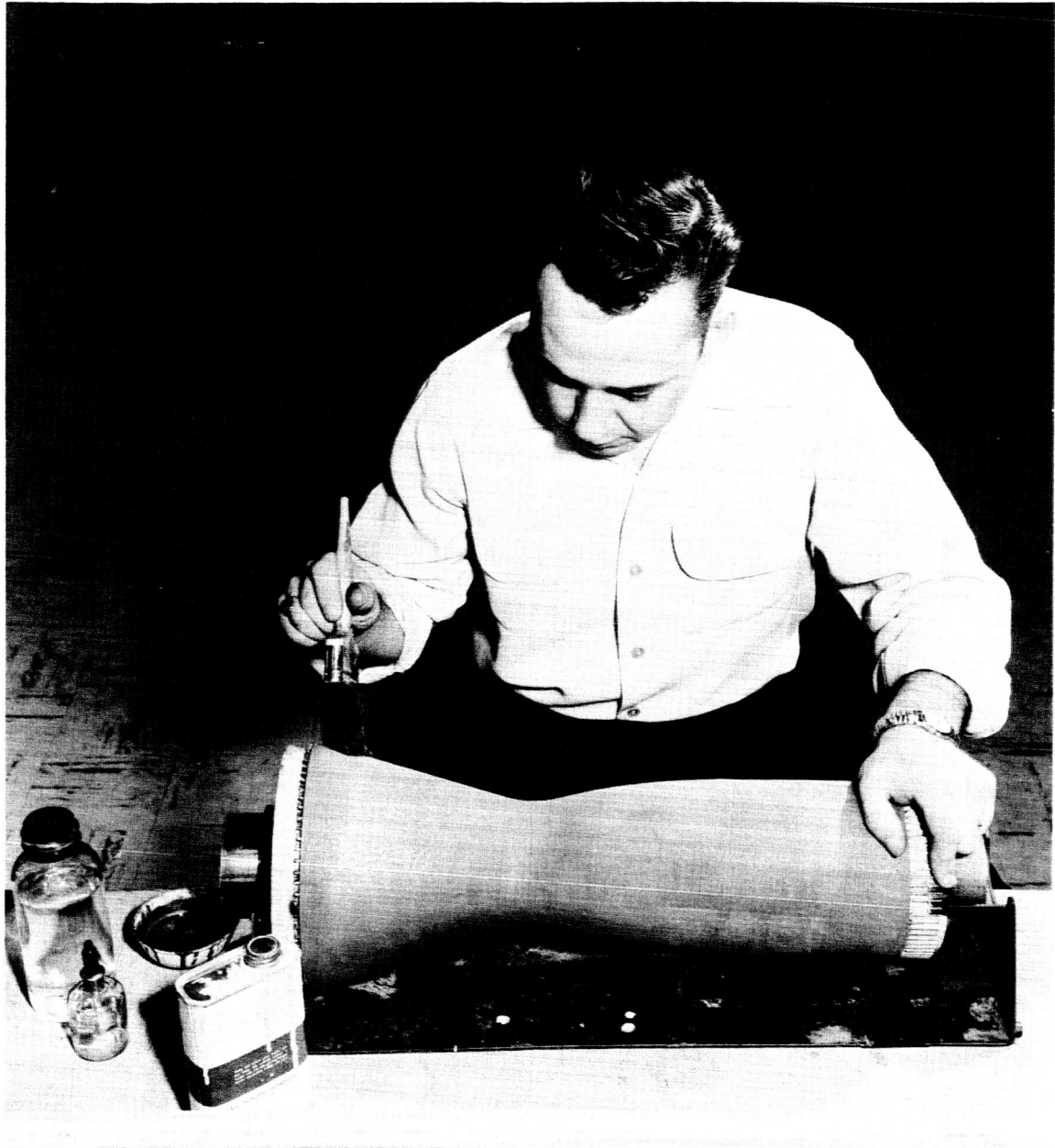
E-183

CK-7

C-47934

Figure 22. - Applying braze to wire-wrapped channel assembly.

Figure 23. - Installing channel assembly in vacuum-brazing furnace.
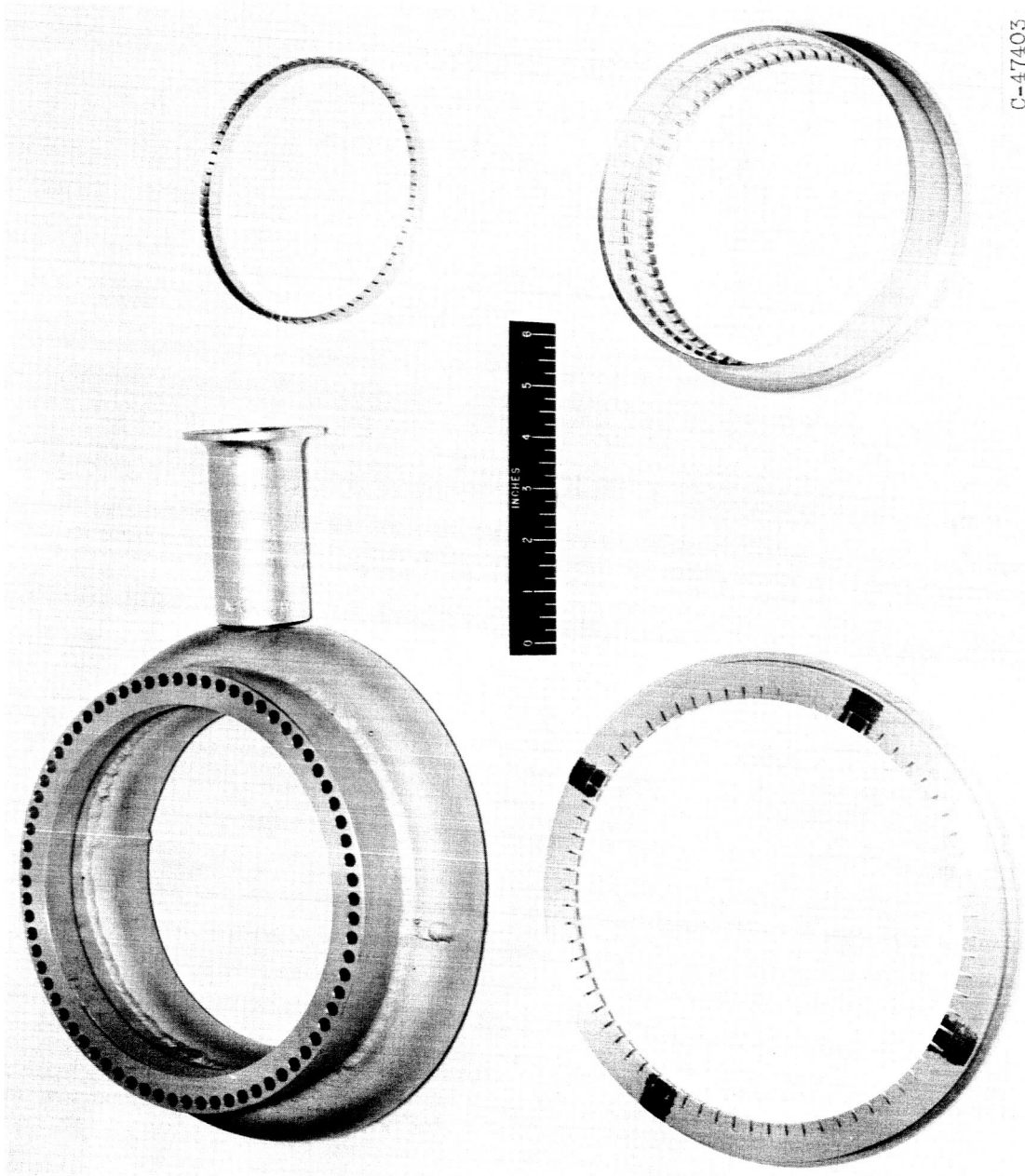
C-47403

Figure 24. - Components to complete thrust chamber.
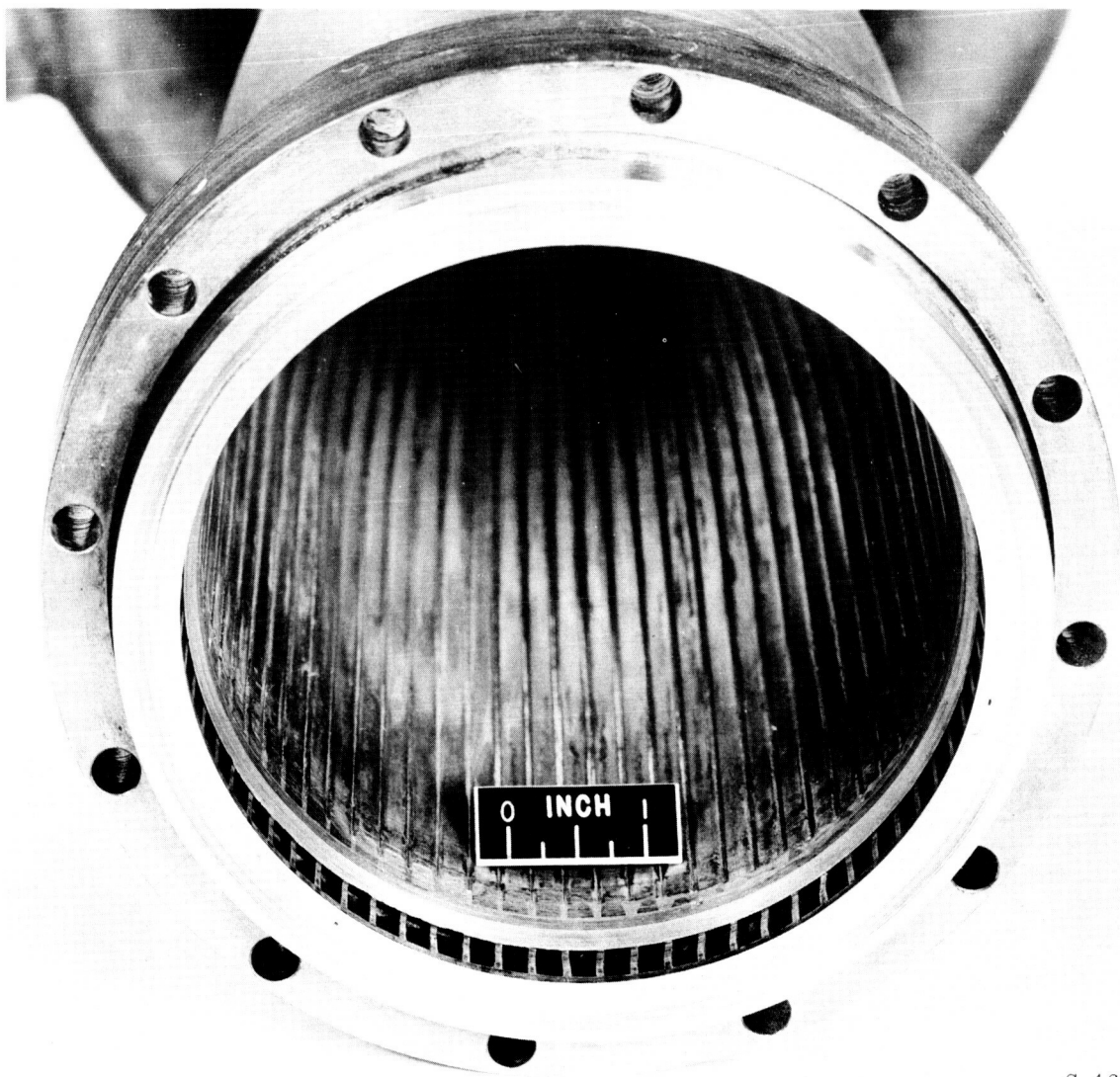
C-46606

Figure 25. - Detailed view of cooling-jacket discharge passages.

E-183
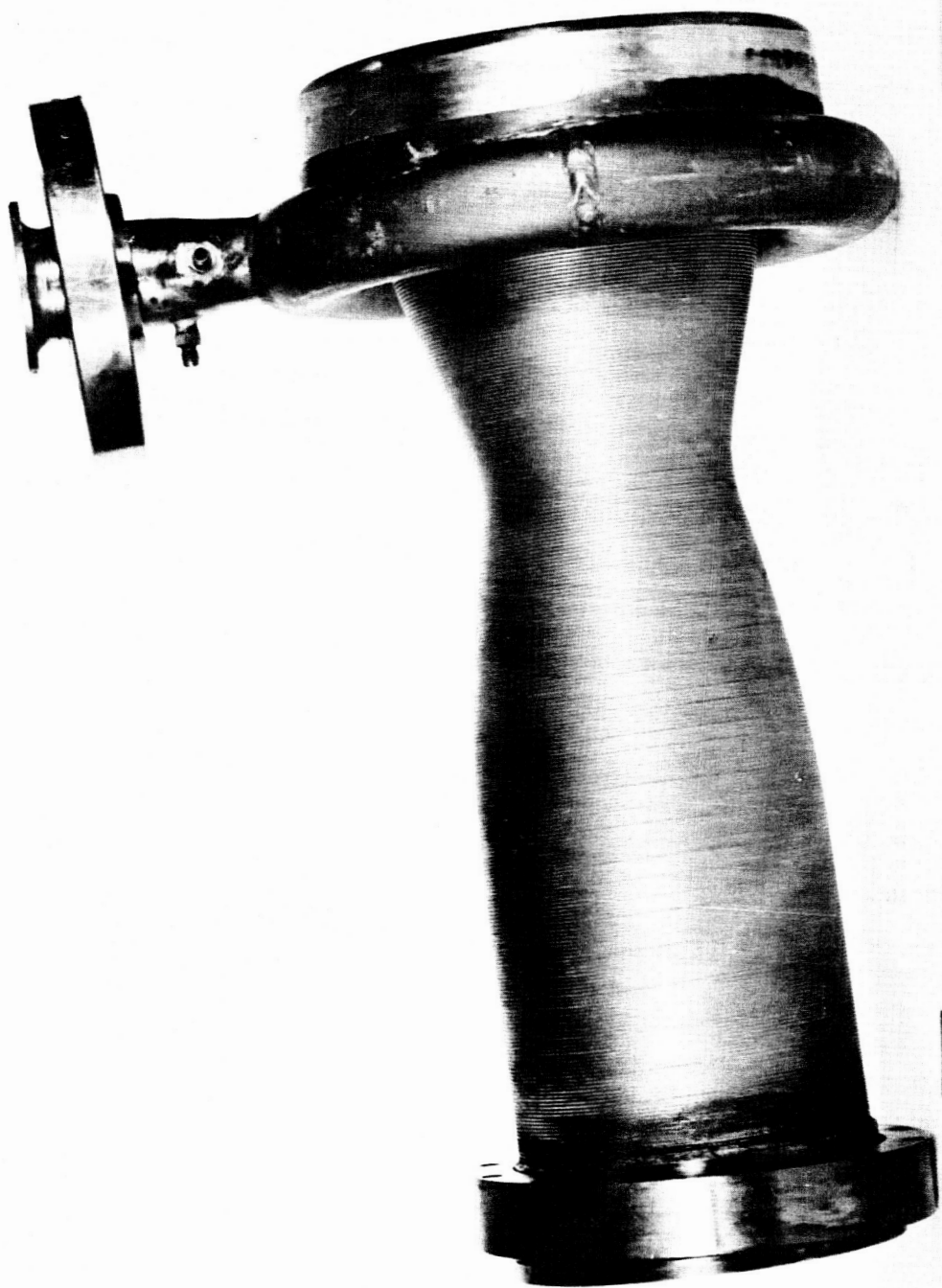
C-46609

Figure 26. - Completed thrust chamber.